



## D8.19 Report on the identification and use of climate change indicators and related impacts change based on the CLIMA VRE



• Deliverable number:	• D8.19
• Work package:	• WP8 – Virtual Research Environments and Cross-disciplinary Activities
• Intermediate Objective:	• IO8.10
• Deliverable type:	• X Document, report
•	• <input type="checkbox"/> Websites, patent filings, videos, etc.
•	• <input type="checkbox"/> Other: please specify .....
• Dissemination level:	• X Public
•	• <input type="checkbox"/> Restricted
• Estimated delivery (bimester):	• B19
• Actual delivery date:	• B19
• Author(s) (Partner-OU):	• Daniele Lagomarsino Oneto, Roberta Sciascia, (CNR-ISMAR Lerici), Marta Falossi, Andrea Valli, Andrea Lira-Loarca, Annalisa Azzola, Giovanni Besio (Università di Genova), Carlo Mantovani and Marcello G. Magaldi (CNR-ISMAR Lerici)
• Reviewed by:	• ITINERIS Executive Board
• Note:	•

IR0000032 – ITINERIS, Italian Integrated Environmental Research Infrastructures System - CUP B53C22002150006 (D.D. n. 130/2022)

Funded by EU - Next Generation EU

Mission 4 “Education and Research” - Component 2: “From research to business” -

Investment 3.1: “Fund for the realisation of an integrated system of research and innovation infrastructures”

---

## Table of contents

1. INTRODUCTION.....	5
<b>Scope and structure of the deliverable .....</b>	<b>5</b>
2. A CLIMATIC INDICATOR FOR THE LIGURIAN SEA .....	6
<b>Climatological parameters included in the Ligurian Sea Climatic Index .....</b>	<b>8</b>
<b>Sea surface temperature .....</b>	<b>9</b>
<b>Marine heat waves.....</b>	<b>9</b>
<b>Marine heatwaves in shallow coastal habitats .....</b>	<b>11</b>
<b>Extension of MHWs in the Ligurian Sea.....</b>	<b>14</b>
<b>In-situ water temperature and salinity.....</b>	<b>14</b>
<b>The Corsica Channel.....</b>	<b>16</b>
<b>The Dyfamed observatory .....</b>	<b>17</b>
<b>The Odis Italia 1 (“W1M3A”) buoy.....</b>	<b>18</b>
<b>The composite indicator: the Ligurian Sea Climatic Index.....</b>	<b>21</b>
3. MARINE INVASIVE SPECIES DISTRIBUTION IN CLIMATE CHANGE SCENARIOS.....	25
<b>Bio-geophysical climate datasets .....</b>	<b>25</b>
<b>Biological datasets .....</b>	<b>28</b>
<b>The machine learning model .....</b>	<b>28</b>
<b>Suitability maps .....</b>	<b>30</b>
4. OTHER APPLICATIONS OF THE CLIMA VRE.....	33
<b>Marine connectivity studies in Tanzania.....</b>	<b>33</b>
<b>A new APP: the Glider Mission Portal.....</b>	<b>41</b>
5. CONCLUSIONS .....	46
6. REFERENCES .....	47

## 1. INTRODUCTION

As well described in the Section 1 of Deliverable 8.13, Virtual Research Environments (VREs) are online collaborative platforms designed to integrate software tools, data, and computational resources into a unified workspace. VREs support their users, mainly researchers, but not only, in finding solutions and addressing scientific and/or management questions (Assante et al., 2023). Being inspired by the Open Science and Findable, Accessible, Interoperable and Reusable (FAIR, Wilkinson et al., 2016) principles, their primary goal is to overcome several challenges in many current research fields, such as data fragmentation, resource limitations, and barriers to collaboration. Following these directions, VREs can be used not only for enhancing collaborations across disciplines but also for managing and analyzing large datasets and for ensuring reproducibility of analyses and obtained results.

Following these directions, Activity 8.7 of the ITINERIS project is focused on developing the so-called “CLIMA VRE”, i.e. a Virtual Research Environment dedicated to the analysis of climatic variables with the specific aim of identifying, developing and implementing new climatic indicators. The CLIMA VRE is dedicated to Climate Change being recognized as a major global challenge, affecting environmental and human systems through rising temperatures, sea-level rise, and extreme weather. The latest “State of the Climate in 2024” report (Blunden and Reagan, 2025) shows that 2024 was the warmest year on record across most continents, including North America, South America, Africa and Europe. Only for Asia 2024 was the second-warmest year on record. Such trends demand collaborative, data-intensive analyses that traditional standalone tools can no longer support. VREs provide this collaborative environment with shared computational resources, standardized workflows, and continuous access to distributed data.

As underlined in Deliverable 8.3, climate indicators are crucial tools for monitoring changes in the Earth’s climate system and for assessing the effectiveness of mitigation and adaptation strategies. Key indicators, such as global temperature, sea-level rise, and greenhouse gas concentrations, provide scientifically robust evidence of climate trends. These metrics also help communicate the urgency of climate action to society, encouraging awareness and behavioral change.

The CLIMA VRE is one of the VREs developed within the ITINERIS project thanks to the D4Science e-infrastructure (Assante et al., 2019; Candela et al., 2023). It uses the ITINERIS VRE Gateway developed specifically for the ITINERIS project, offering customized tools for data analysis and visualization. Through the D4Science Identity and Access Management system, users can log in and access their personal dashboard. The interface provides direct links to shared workspace and messaging services. The reader is referred to Deliverable 8.13 which represents the CLIMA VRE User Guide for a detailed description of its functionalities.

### **Scope and structure of the deliverable**

This Deliverable D8.19, together with D8.17, D8.18, D8.20 and D8.21, supports the Intermediate Objective IO8.10 of ITINERIS and demonstrates the full operativity of the CLIMA VRE, a key objective (OBJ7) of the WP8 “Virtual Research Environments and Cross-disciplinary Activities”. The document is organized in several Sections: Section 2 presents the creation of a new composite climatic indicator, the Ligurian Sea Climatic Index; Section 3 illustrates the use of the CLIMA VRE to predict invasive-species distribution under climate change scenarios; Section 4 shows its application to particle-dispersion simulations for marine connectivity in Tanzania and to the development of a Glider Mission Portal App. The final Section 5 provides the conclusions.

## 2. A CLIMATIC INDICATOR FOR THE LIGURIAN SEA

In this section of the Deliverable it is shown how the CLIMA VRE has been used for the definition of a composite climatic index for the Ligurian Sea, the Ligurian Sea Climatic Index (LSCI). All components of the LSCI originate from physical variables which are known to drive and impact human activities and ecological processes.

Following the guidelines of the World Meteorological Organization (WMO 2017), the physical variables are indicated as “elements” in the LSCI definition while the derived statistical descriptors are treated as “parameters”. The LSCI then aggregates multiple information from physical elements and derived parameters which are evaluated in the context of the Ligurian Sea. Moreover, to capture and resolve processes peculiar of this area, all LSCI variables are either within the Essential Climate Variables (ECV) framework (Bojinski et al. 2014; WMO et al. 2025) or directly derived from ECVs. The reader is referred to the Deliverable 8.3 for a more detailed description of the ECVs framework.

More specifically, the following elements and parameters have been analysed for the LSCI definition: the behavior of the sea surface temperature (SST); the occurrence of marine heatwaves (MHW) and the resulting thermal stress (THS), along with the extent of the Ligurian Sea domain affected by these events; the behavior of in-situ temperature, salinity and the Levantine Intermediate Water (LIW) size at the Corsica Channel, at the Dyfamed observatory and at the Odas Italia 1 (“WIM3A”) buoy.

Data of diverse origin have been processed, from remote and in-situ observations to three-dimensional (3D) gridded variables available in reanalysis products. The derived parameters are of diverse nature: some are meant for summarizing properties of the whole domain, others look for local variations. Moreover, in some cases they have been chosen to follow large-scale trends, in other cases they focus on extreme events (e.g. heatwaves). All these aspects are to date recognized as relevant for tracking climate variability.

Climatic indicators aim at synthesizing variations which are related to a specific area or a particular process, and many of them have been developed in the past (see Deliverable 8.3 for a comprehensive list and review). A standard approach is to evaluate how climatic parameters deviate from their “normal” behavior, where the word “normal” indicates typical values showed by a parameter during a reference period. In a system undergoing rapid changes, clearly defining what is considered “normal” becomes essential. For instance, the latest update to the WMO guidelines on climate normals has shifted the recommended reference period from fixed, non-overlapping 30-year intervals to a rolling window covering the most recent three full decades (currently 1991–2020, WMO 2017). Nevertheless, the challenge of defining appropriate climatological normals continues to be widely debated, particularly as more advanced and methodologically diverse approaches emerge in the scientific literature. The reader can consult Rigal et al. (2019) for illustrative examples of alternative and increasingly sophisticated techniques.

The idea behind the Ligurian Sea Climatic Index follows the line of thought of Cyr and Galbraith (2021) for designing a climatic indicator of Newfoundland and Labrador Sea. In this approach each component of the LSCI might be thought as a climatic index *per se*, defined as an anomaly, i.e. the deviation of a parameter from its climatological normal. The procedure to compute each anomaly is detailed case by case in the following paragraphs.

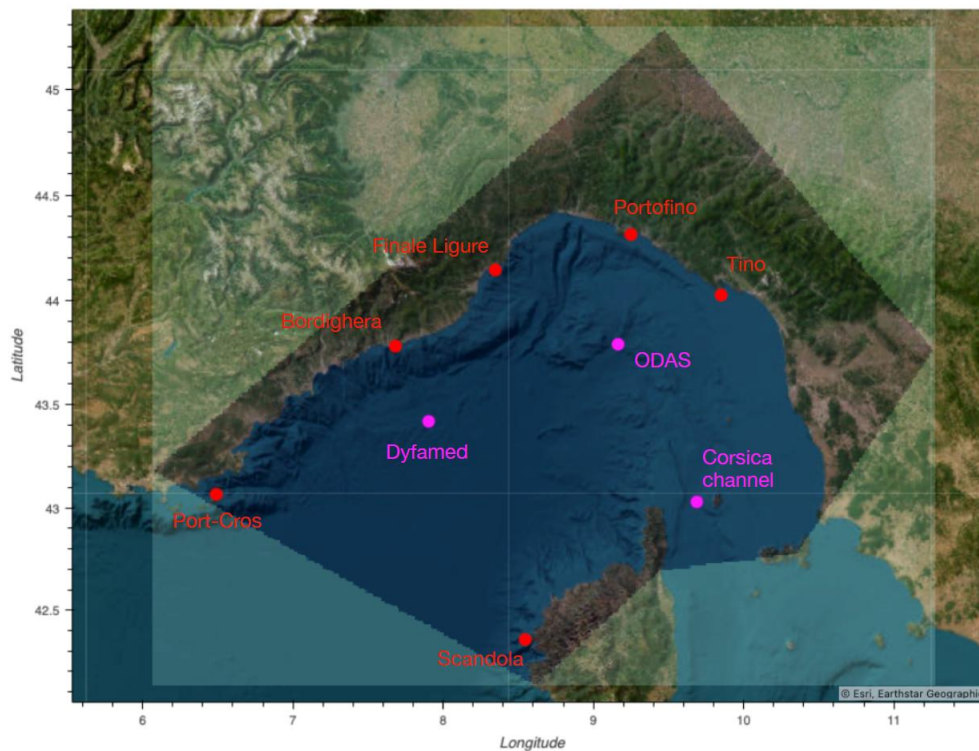


*Figure 1: Area of application of the Ligurian Sea Climatic Index. The mask used to cut gridded variables is defined as the intersection between the dark shaded polygon and the sea points of the data grid. Virtual moorings are indicated as purple dots and corresponds to active observational facilities which are already working in the Ligurian domain (the Corsica Channel mooring, the ODAS Italia 1 “WIM3A” buoy and the Dyfamed observatory). Coastal locations where significant mass mortality events were recorded in previous studies are also indicated as red dots.*

*Table 1 – Geographical locations defining the polygon that has been used for building the Ligurian sea mask.*

Location	Latitude (°N)	Longitude (°E)
Toulon	43.182	6.070
The Po Valley	45.284	9.473
Florence	43.765	11.267
Elba Island	42.782	10.358
Bastia	42.699	9.450
Cargèse	42.137	8.620

### Climatological parameters included in the Ligurian Sea Climatic Index

Before examining the details of each parameter, it is useful to highlight some general considerations. With respect to the time dimension, the WMO guidelines (WMO 2017) provide recommendations for computing climatological normals at different temporal resolutions (monthly, seasonal, and annual) and for various types of parameters (averages, extremes, counts, and cumulative quantities). Although the most recent update of these guidelines does not explicitly address this point, a growing practice in the literature is to also consider daily anomalies based on calendar-day normals. This approach is particularly relevant when dealing with extreme events, which typically take place over short time scales. For this reason, the Ligurian Sea Climatic Index adopts daily-based parameters in specific cases. Nevertheless, unless otherwise stated, to ensure consistency with WMO recommendations, daily time series have been aggregated to monthly or annual values in the following paragraphs.

With respect to the spatial scales, when computing statistics over the full domain, the gridded datasets have been first restricted to the Ligurian Sea area (Figure 1), defined as the region contained within the polygon of geographical coordinates listed in Table 1.

In certain cases, in-situ observations have been reproduced by sampling reanalysis fields at the locations of existing observational platforms whose records do not meet the minimum 30-year requirement established by the WMO guidelines. In the following paragraphs, for each physical variable included in the LSCI, the corresponding data sources are described together with the associated applied processing procedure.

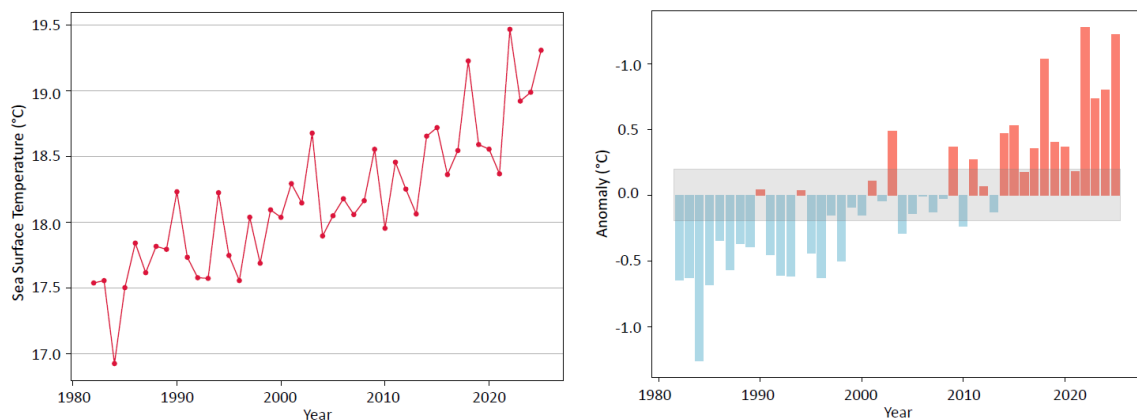


*Figure 2: Domain-averaged SST (left panel) and associated annual anomalies (right panel). Zero-anomaly values correspond to years in which the annual mean equals the climatological mean computed over the 1991–2020 period. The grey band on the right panel is centered on zero and spans one standard deviation above and below the climatological mean.*

### **Sea surface temperature**

As underlined in Deliverable 8.3, the sea surface temperature (SST) is considered as an essential climate variable not only for its fundamental role within the marine environment but also as it directly affects both the atmospheric circulation and the precipitation field. Leveraging mainly on satellite data, SST datasets are also among the most robust and reliable sources of information for the estimations of the global and regional temperature fields. The same first App of the CLIMA VRE, the Italian Sea surface temperature demonstrator (ISSTD) App, introduced already in Deliverable 8.13, is based on the calculations of SST anomalies for the four main Italian Seas. In this Deliverable 8.19, the behavior of SST is assessed at the regional scale of the Ligurian Sea by averaging over the entire domain as described in the previous paragraph.

Data from the Mediterranean Sea – High Resolution L4 Sea Surface Temperature Reprocessed dataset (EU-CMEMS 2026a), openly accessible through the Copernicus Marine Data Store, have been employed. This dataset provides reliable daily (nighttime) SST time series from January 1, 1981 to the present. The fields are produced through optimal interpolation (L4 processing level) of satellite-derived estimates of the foundation SST (i.e., temperature free or nearly free of any diurnal cycle) onto a 0.05°-resolution grid covering the Mediterranean Sea and part of the adjacent North Atlantic Ocean. After the application of the Ligurian Sea mask, domain-averaged daily SST values have been obtained by computing the area-weighted mean across all ocean grid points.

Monthly means have been then calculated starting from the daily values. The resulting monthly time series have been used to evaluate the SST climatological normal for the reference period 1991–2020 as recommended by the WMO guidelines (WMO 2017). Annual series and their corresponding climatological normals have been subsequently obtained by aggregating monthly mean values belonging to the same calendar year (Figure 2).

The SST anomaly trend represents the first LSCI component and exhibits a persistent warming trend (Figure 2), consistent with the pattern observed at global scales (C3S, 2025).

### **Marine heat waves**

To date, the accelerating trend of global warming, particularly in the oceans, represents a clear manifestation of ongoing climate change. However, average warming trends capture only one dimension of how climate change has altered Essential Climate Variables in recent decades. Extreme events, for example, have drawn significant attention because of their ecological consequences. While many species may cope with gradual environmental changes, the intense stress imposed by extreme events, even when limited in space and time, can threaten the same species survival. For this reason, the LSCI definition includes a specific component to describe extreme water-temperature events that exert thermal stress on a wide range of organisms: the Marine Heatwaves (MHWs).

Although MHWs can be defined based on species-specific thermal tolerances, in this Deliverable 8.19, an ecosystem-independent definition, which does not rely on biological characteristics, is adopted. Following Hobday et al. (2016, 2018), extreme sea-surface temperature (SST) values at each grid point are identified using calendar-day climatological percentiles. For each calendar day  $d$  (from 1 to 366), a temporal window of half-width  $D$  days centered on day  $d$  is considered. The procedure, illustrated in Figure 3, can be summarized with the following steps:

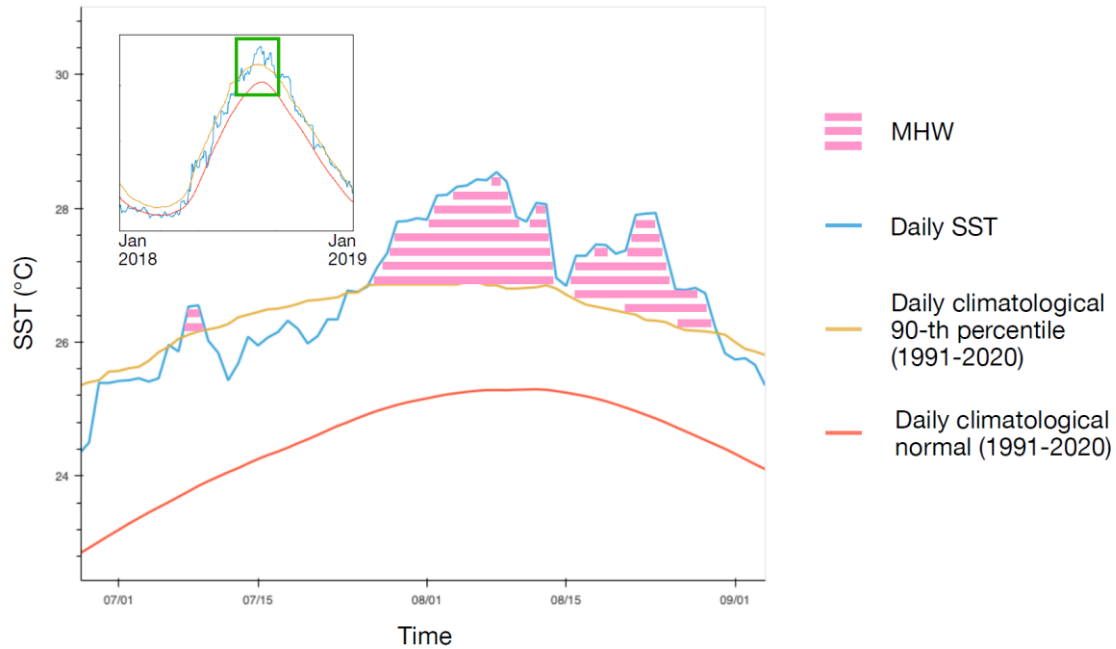


*Figure 3: Marine Heatwaves (MHW) identification procedure. At each grid point, the climatological 90th percentile of SST for each calendar day (yellow line) is used as a dynamic threshold for classifying SST values (light-blue curve) as normal or extreme (highlighted in pink). Consecutive extreme periods are subsequently filtered or merged according to their duration or separation in time. The resulting binary time series of MHW occurrence is then used to compute the metrics associated with MHWs.*

- for each window centered on calendar day  $d$ , SST values are collected from all years in the reference period 1991–2020 that fall within the window;
- the 90th percentile ( $p90_d$ ) of this distribution is then computed;
- at each grid point, a heatwave is defined as any period in which  $SST_{d,y} \geq p90_d$  for at least five consecutive days (where  $d$  and  $y$  denote day and year, respectively);
- heatwave events that are separated by fewer than two days are eventually merged.

It is important to note that the climatological percentile used in the MHW definition is not intended to represent a climatological normal; rather, it is a fundamental component of the definition of this extreme physical element. Nonetheless, for consistency, the climatological percentiles are here computed using only data from the same reference period used for the climatological normals.

After identifying MHWs, two separate analyses have been carried out. First, indicators related to the potential impact of MHWs on coastal habitats have been considered. Second, the spatial extent of MHWs within the Ligurian Sea domain has been assessed. These analyses are described in the next paragraphs.

*Table 2 – Geographical coordinates and names of the coastal sites selected for monitoring MHWs.*

<b>Location</b>	<b>Latitude (°N)</b>	<b>Longitude (°E)</b>
Port-Cros	43.066	6.490
Portofino Cape	44.313	9.250
Finale Ligure	44.144	8.347
Scandola	42.357	8.546
Tino Isle	44.025	9.850
Bordighera	43.780	7.682

### **Marine heatwaves in shallow coastal habitats**

A few coastal sites in the Ligurian Sea have been selected to account for the impact of MHWs on shallow-water ecosystems. These locations correspond with the geographical areas where severe damages to numerous marine species associated with MHWs have been reported (Cerrano et al., 2000; Garrabou et al., 2021; Toma et al., 2022). Remarkable examples are the mass mortality events affecting coralligenous species, which are recognized as habitat-forming organisms (Estaque et al., 2023). The coordinates of the selected coastal sites are provided in Table 2.

Several characteristics have been computed for each detected MHW; examples include the duration (i.e., the number of days the event persists), the cumulative thermal stress (obtained by integrating SST values over the entire heatwave duration), and the average SST value recorded during the event. Specifically, for every MHW detected at each coastal site, thermal heat stress (THS) has been defined by multiplying the event duration by the maximum measured SST value. The ensemble average has been then used as the statistical parameter associated with the derived climatic indicator. Ensembles have been constructed by aggregating MHW events identified at each coastal site within each temporal interval considered for the definition of the processed time series.

Furthermore, since the focus of the analysis are the ecological impacts of MHWs and the most severe events generally occur in late summer and early autumn, the observational period has been restricted to June through November. To implement this constraint, as MHWs by definition span multiple days, each MHW has been assigned to the month in which the majority of its duration occurs.

Figures 4, 5, and 6 illustrate the behavior of THS at all selected locations. As also indicated by the aggregated normalized anomaly across all coastal sites (Figure 7), a common pattern emerges despite some location-specific differences: an increased occurrence of MHWs has been observed after the year 2000, accompanied by higher levels of thermal stress. An exceptionally high thermal stress is recorded at all sites in 2024.

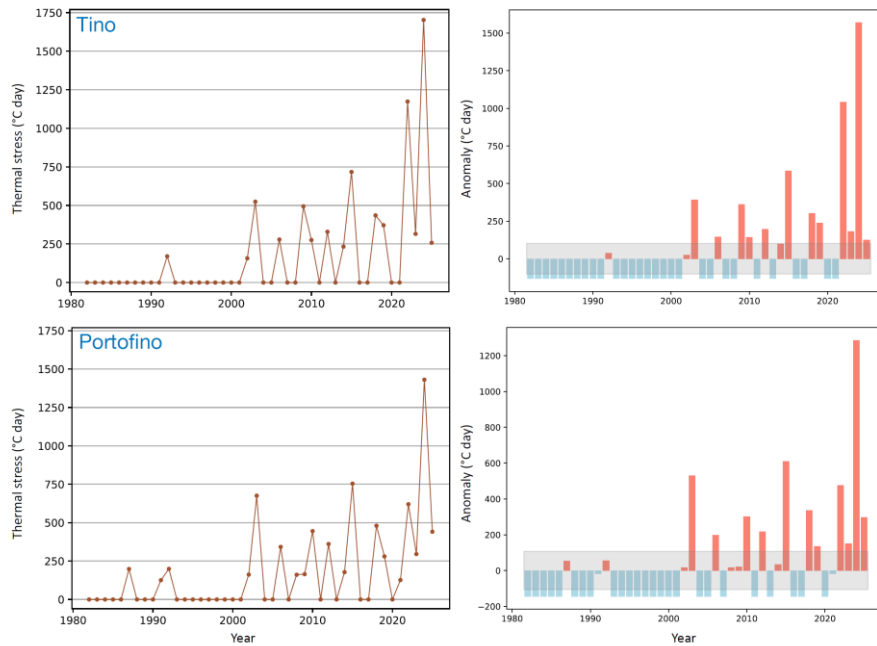


*Figure 4: Thermal stress associated with MHWs at the Tino Isle (top left) and Portofino Cape (bottom left) locations with their respective annual anomalies (top right and bottom right). Zero-anomaly values correspond to years in which the annual mean equals the climatological mean computed over the 1991–2020 period. The grey bands on the right panels are centered on zero and span one standard deviation above and below the climatological mean.*

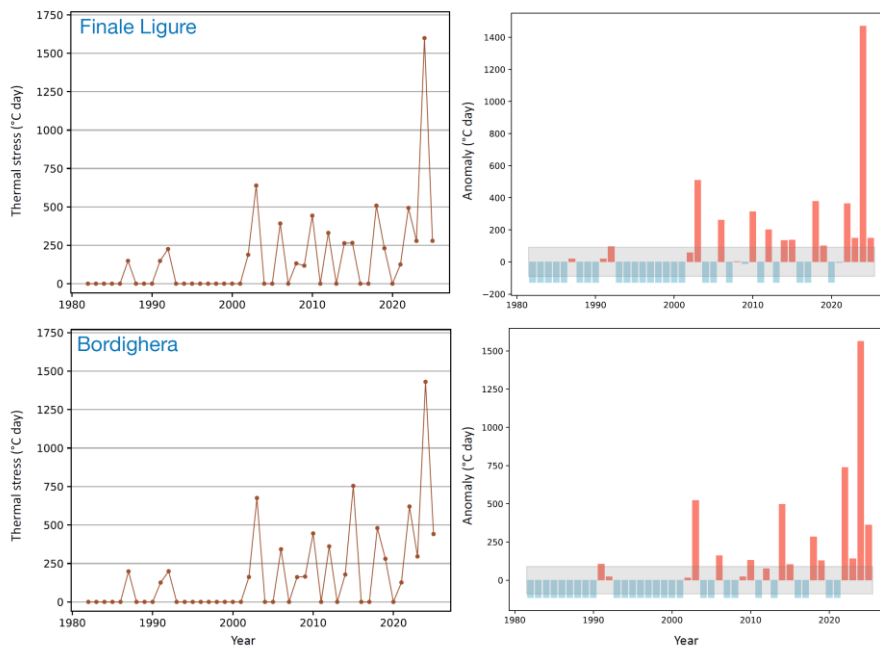


*Figure 5: As in Figure 4 but for the Finale Ligure and Bordighera locations.*

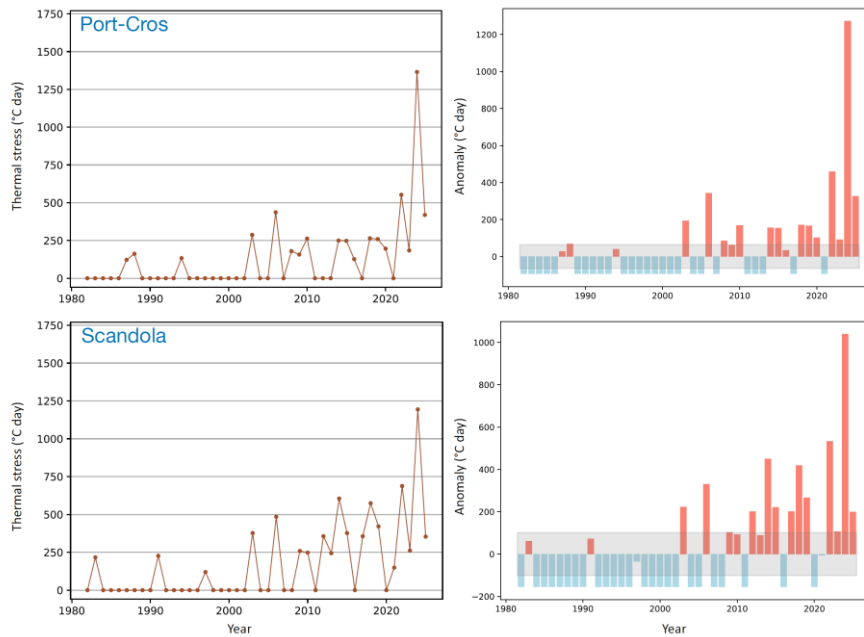


Figure 6: As in Figures 4 and 5 but for the Port-Cros and Scandola locations.

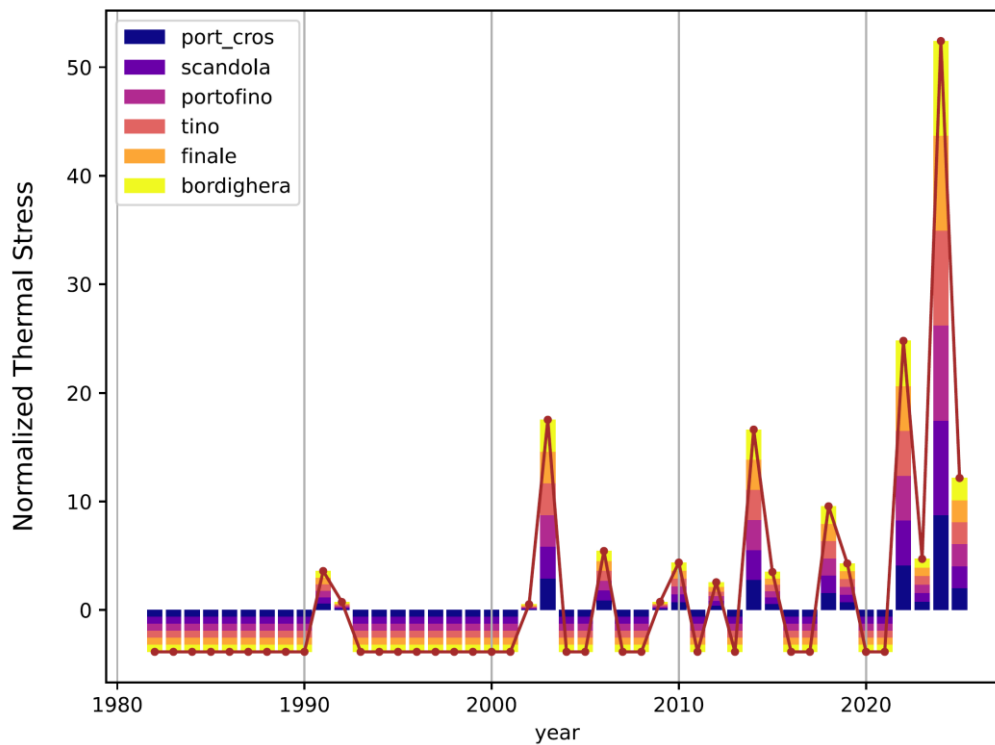
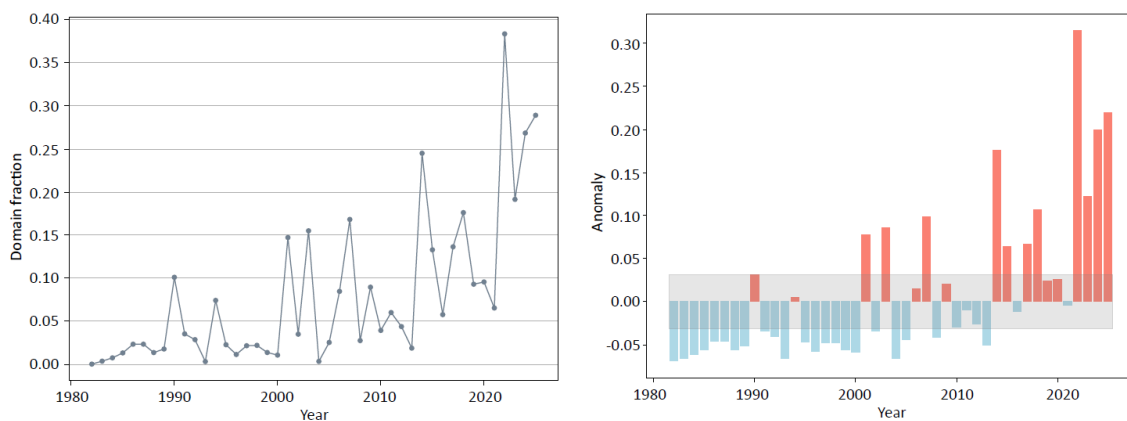


Figure 7: Normalized anomalies (anomalies divided by their respective standard deviations) of thermal stress at all six coastal locations, averaged together in a unique index.

### Extension of MHWs in the Ligurian Sea

A second MHW-related analysis has been considered in building the LSCI: the geographical extent of the heatwaves. This extent has been quantified after the MHWs identification over the entire domain and by calculating the fraction of the Ligurian Sea surface affected by a MHW event on a daily basis. This fraction has been obtained by weighting each grid point by its corresponding area, which depends on the angular grid spacing and latitude, followed by the normalization with respect to the total sea surface. The resulting variable, *Domain Fraction*, assumes values between 0 and 1, where 0 indicates the absence of MHWs and 1 indicates that the entire domain is experiencing a MHW.

Figure 8 shows an increasing trend for this variable, consistent with the behaviour of other SST-derived parameters. However, unlike thermal stress, the most severe year in terms of MHW spatial extent is 2022.



*Figure 8: Fraction of the Liguria Sea subjected to MHWs (left) and its annual anomaly (right). Zero-anomaly values correspond to years in which the annual mean equals the climatological mean computed over the 1991–2020 period. The grey band on the right panel is centered on zero and spans one standard deviation above and below the climatological mean.*

### In-situ water temperature and salinity

SST trends and variables associated with extreme surface and coastal events do not provide any information on the internal state of the Ligurian Sea. To include this information in the LSCI, attention has been put on three observational sites where physical oceanographic variables are already monitored: the Corsica Channel mooring, the Odas Italia 1 (“W1M3A”) buoy, and the Dyfamed observatory (see Figure 1 and Table 3 for their locations). However, data from reanalysis products interpolated at the corresponding geographical positions has been preferred with respect to observations since the datasets provided by these facilities are heterogeneous and sometimes limited in temporal coverage. For this reason, these sites are referred to as “virtual” moorings. The rationale behind this choice is two-fold. On one hand it is based on the fact that observational datasets are incorporated into reanalysis products through data-assimilation techniques, allowing the model fields to be continuously corrected toward measured conditions. Because these observations actively

constrain the model, the resulting reanalysis fields should not diverge significantly from real measurements. In this way, reanalysis products provide spatially and temporally complete datasets that remain physically consistent and tightly anchored to actual observations.

On the other hand, the same choice relies on the considerable effort invested in recent years by the scientific community to organize, standardize and enhance data acquisition and quality assurance. The expectation is that these “virtual” moorings may eventually be replaced, at least partially, by direct observations in the future.

Data from the Mediterranean Sea Physics Reanalysis dataset (EU–CMEMS 2026b), openly accessible through the Copernicus Marine Data Store, have been employed for this purpose. This reanalysis product provides a high-resolution multidecadal reconstruction of the physical state of the Mediterranean Sea, integrating ocean modelling and advanced data assimilation. Its core is the NEMO (Nucleus for European Modelling of the Ocean) hydrodynamic model, a state-of-the-art primitive-equation framework widely used in climate and operational oceanography (Madec and the NEMO System Team, 2024). The system is coupled with OceanVAR, a three-dimensional variational (3D-VAR) data assimilation scheme specifically developed for the Mediterranean Sea, which assimilates in-situ temperature and salinity profiles together with satellite altimetry to optimally constrain the model fields (Dobricic and Pinardi, 2008). Running at 1/24° horizontal resolution and employing 141 vertical levels, the reanalysis resolves mesoscale structures and the complex stratification of the basin with high fidelity. The dataset is updated annually and complemented with interim monthly extensions, ensuring continuity up to approximately one month before present. Thanks to the assimilation of extensive satellite and in-situ measurements, the reanalysis is ideal for LSCI-related analyses as it maintains high realism while offering full spatial and temporal coverage.

At each location, vertical profiles of potential temperature and practical salinity have been extracted from surface to seabed by linearly interpolating the scalar fields provided by the reanalysis at its 141 vertical fixed z-levels (constant depth). Consequently, the number of values in each profile varies according to the local bathymetry. Potential temperature has been subsequently converted into in situ temperature using functions from the Python Gibbs Seawater toolbox, an implementation of the Thermodynamic Equation of Seawater (TEOS-10, McDougall and Barker, 2011).

*Table 3 – Geographical coordinates and names of the three virtual moorings used in the LSCI.*

<b>Virtual Mooring</b>	<b>Latitude (°N)</b>	<b>Longitude (°E)</b>
Corsica Channel mooring	43.029	9.688
Dyfamed observatory	43.418	7.903
Odas Italia 1 (“W1M3A”) buoy	43.789	9.164

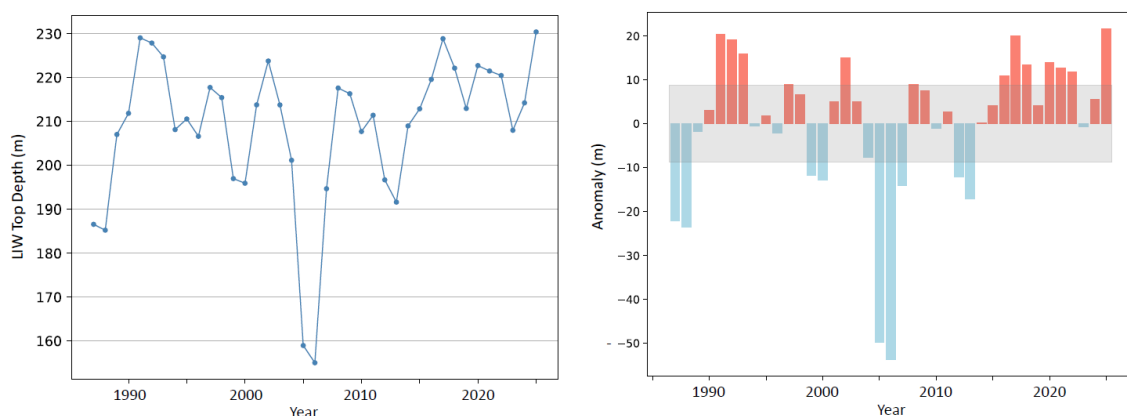
### The Corsica Channel

The Corsica Channel is a relatively narrow (~32 km) oceanic passage through which the Ligurian and Tyrrhenian basins are connected. It is situated between the northeastern tip of Corsica and the Capraia Island, and reaches a maximum depth of approximately 430 m. It is regarded as a key site for the exchange of water masses, particularly for the dense waters originating in the Eastern Mediterranean, traditionally referred to as Levantine Intermediate Water (LIW), although its definition and evolution remain the subject of scientific debate (see for example Millot, 2013).

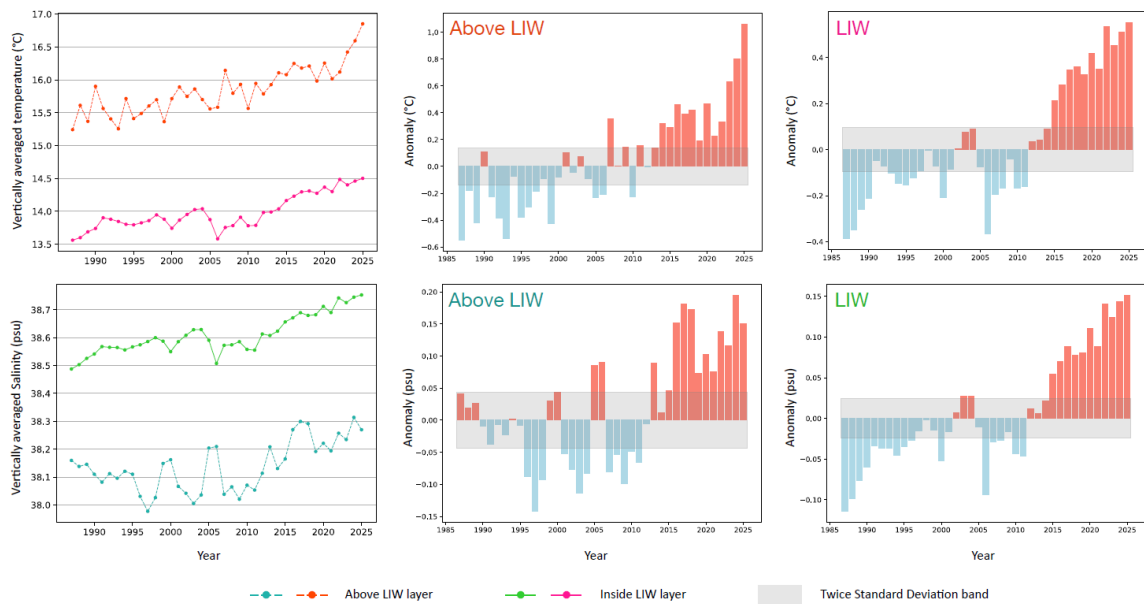
For the purpose of identifying the denser intermediate waters transiting through the channel, the upper boundary of this layer (“LIW top”) has been estimated as the shallowest depth at which the potential density referenced to the surface ( $\sigma_\theta$ ) exceeds the  $28.9 \text{ kg m}^{-3}$  value, a threshold already associated with LIW in previous studies (Sciascia et al., 2019). Vertical profiles of in-situ temperature and salinity are subsequently averaged above and below this dynamically varying depth, effectively treating the water column as a two-layer system. Using this procedure, five different physical variables have been included in the LSCI for the Corsica Channel: the salinity and in-situ temperature for the LIW layer, the salinity and in-situ temperature for the layer above the LIW, and the LIW layer thickness.

Figure 9 displays the annual evolution of the LIW-top depth, which fluctuates around the climatological mean without exhibiting a clear long-term trend. Nevertheless, pronounced negative anomalies are detected in 2005 and 2006, with the LIW top reaching its shallowest levels, less than 160 m, within the analyzed multi-decadal period.

Figure 10 presents temperature and salinity for both the upper (surface to LIW top) and the LIW layers. All variables show a marked increasing trend from the early 2000s onward, with the LIW layer displaying less interannual variability than the upper layer. The stronger oscillations seen in the upper layer are likely attributable to atmospheric forcing and freshwater inputs from land.



*Figure 9: Depth of the upper boundary of the LIW layer (“LIW top”) at the Corsica channel (left) and its annual anomaly (right). Zero-anomaly values correspond to years in which the annual mean equals the climatological mean computed over the 1991–2020 period. The grey band on the right panel is centered on zero and spans one standard deviation above and below the climatological mean.*



*Figure 10: Upper row: vertically averaged in-situ temperature above the LIW layer (orange curve, left panel) and within the LIW layer (pink curve, left panel) at the Corsica Channel, together with their respective annual anomalies (central and right panels) at the same location. Lower row: vertically averaged salinity above the LIW layer (green curve, left panel) and within the LIW layer (blue curve, left panel) at the Corsica Channel, along with their corresponding annual anomalies (central and right panels) at the same location. Zero-anomaly values correspond to years in which the annual means equal the climatological mean computed over the 1991–2020 period. The grey bands on the central and right panels are centered on zero and span one standard deviation above and below the climatological mean.*

### **The Dyfamed observatory**

The Dyfamed (Dynamique des Flux Atmosphériques en Méditerranée) observatory consists of a surface buoy deployed in 1999 while its deep mooring has been operating since 1988 together with regular ship-based campaigns. A combination of near-real-time transmissions and periodically recovered datasets provides surface, deep-water, and atmospheric measurements. Contrarily to the Corsica Channel, the observatory lies in the interior of the Ligurian Sea and is primarily dedicated to the monitoring of water-mass properties and biological exchanges between its eastern and western portions.

The two-layer representation applied in the Corsica Channel has been considered inadequate to describe the presence of deeper and denser layers at the Dyfamed site. Nevertheless, a simplified description remains necessary to condense the complex local dynamics into a limited set of parameters suitable for inclusion in the composite Ligurian Sea Climatic Index. For this purpose, a three-layer structure is adopted, with the LIW acting as the intermediate layer that separates the upper waters (above LIW) from the deeper waters (below LIW). Two dynamically varying depths, the LIW top and LIW bottom, have been defined in analogy with the Corsica Channel approach, but using reference potential density values computed relative to the surface of:

$$\sigma_0^{top} = 28.95 \text{ kg m}^{-3} \text{ and } \sigma_0^{bot} = 29.115 \text{ kg m}^{-3}.$$

These reference densities were proposed by Mallil et al. (2022) for identifying the LIW layer in the Western Mediterranean and differ from the Corsica Channel values. The choice is justified since the LIW layer modifies its physical properties while spreading from its formation regions and a precise definition of its upper and lower boundaries in any region can be non trivial.

Figure 11 illustrates the temporal evolution of the LIW-top and LIW-bottom depths at the Dyfamed observatory, while the LIW-layer thickness is defined as the difference between these two depths. As observed in the Corsica Channel, the year 2006 exhibits a pronounced negative anomaly, linked to an exceptional upward displacement of deep waters. This signal is consistent with documented modifications of the Western Mediterranean thermohaline circulation over recent decades (Schröder et al., 2006).

The long-term trends in water temperature at the Dyfamed observatory are all increasing (Figures 12). Salinity shows an analogous trend (Figure 13), in line with earlier studies highlighting the ongoing warming and salinification of the Mediterranean basin (Schröder et al., 2010; Borghini et al., 2014).

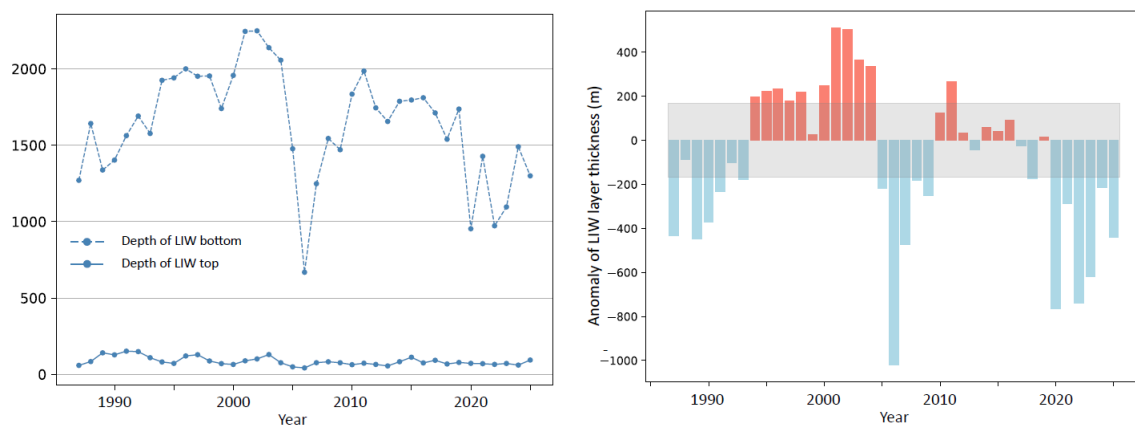


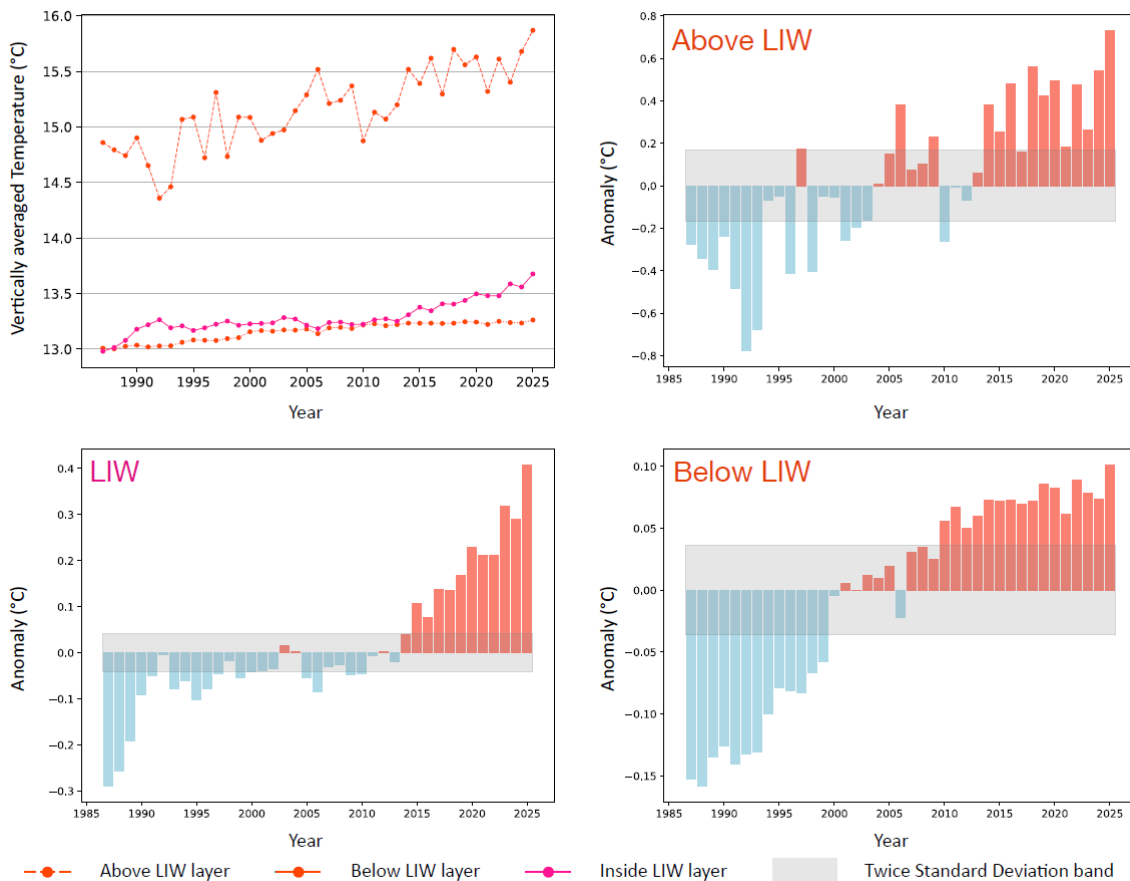
*Figure 11: Depth of the upper and lower boundaries of the LIW layer (“LIW top” and “LIW bottom”) at the Dyfamed observatory (left) and annual anomaly of the LIW layer thickness at the same location (right). Zero-anomaly values correspond to years in which the annual mean equals the climatological mean computed over the 1991–2020 period. The grey band on the right panel is centered on zero and spans one standard deviation above and below the climatological mean.*

### **The Odas Italia 1 (“W1M3A”) buoy**

The Oceanographic Data Acquisition System (ODAS) Italia 1 buoy, is actually a part of the Western Mediterranean “W1M3A” observing system. Designed as a large, highly stable spar buoy, it has been operating since 2000 about 80 km offshore in the Ligurian Sea, where it continuously acquires meteorological data and ocean measurements down to 1200 m. Measuring Essential Climate Variables, the buoy contributes to long-term, high-quality observations of air–sea interactions, physical oceanography, and biogeochemical variability. It also provides year-round time-series essential for assessing climate-driven changes such as warming, salinification, and ocean

acidification. Its strategic location in a dynamically active region, characterized by a quasi-permanent cyclonic circulation, makes the buoy particularly valuable for detecting shifts in water-mass properties and circulation patterns linked to climate change. It thus offers one of the most comprehensive long-term marine datasets in the Western Mediterranean.

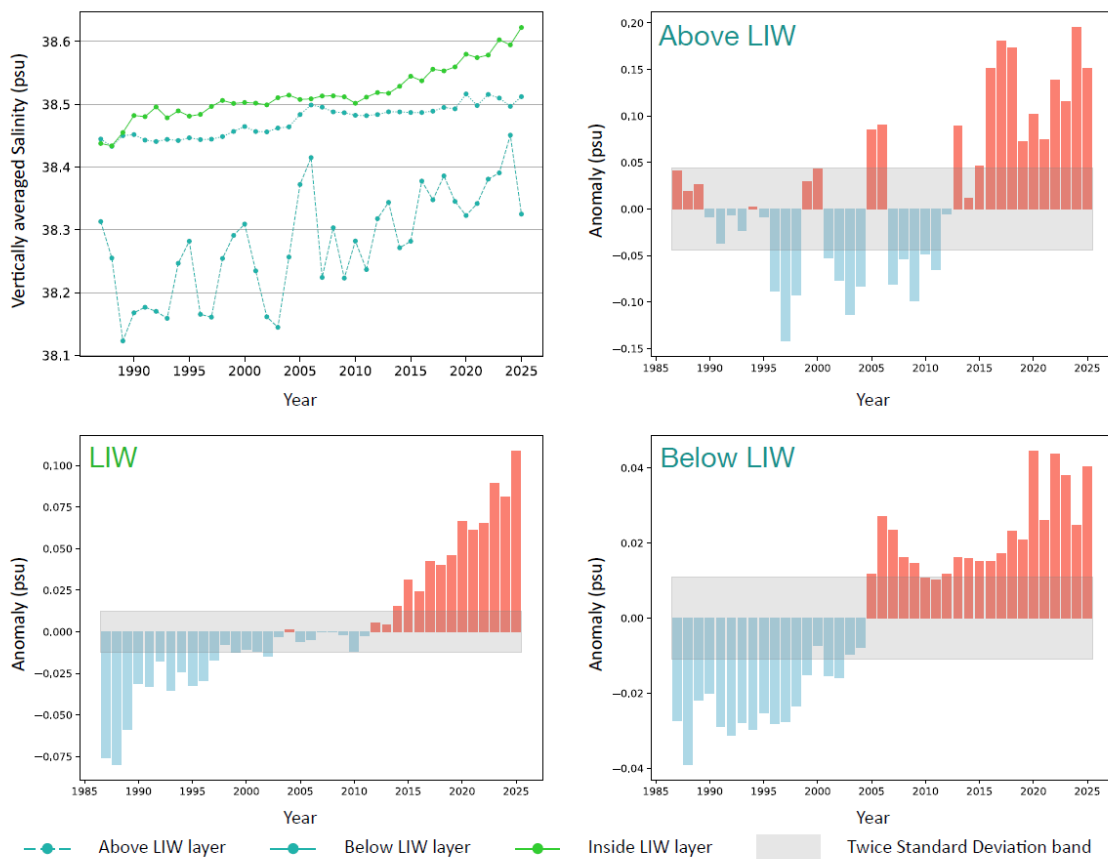
The same approach employed at the Dyfamed observatory has been used also for the variables at the Odas Italia 1 (“W1M3A”) buoy. More specifically, the same three layer representation together with the same reference densities proposed by Mallil et al. (2022) have been applied to the data processing at this location.



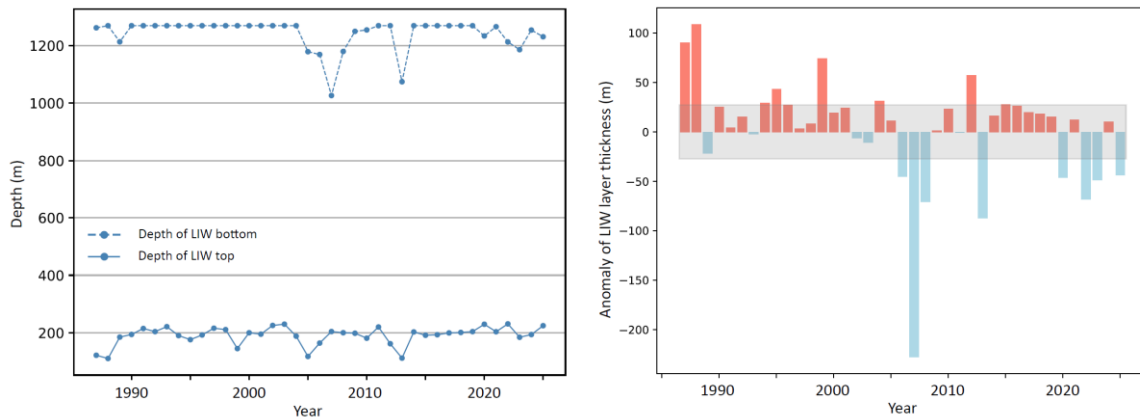
*Figure 12: Vertically averaged in-situ temperature above, inside and below the LIW layer (dashed orange, solid pink and solid orange lines in the upper left panel, respectively) at the Dyfamed observatory and their annual anomalies (upper right, lower left and lower right panels, respectively) at the same location. Zero-anomaly values correspond to years in which the annual means equal the climatological means computed over the 1991–2020 period. The grey bands on upper right, lower left and lower right panels are centered on zero and span one standard deviation above and below the climatological means.*

Figure 14 shows that the temporal evolution of the LIW-top and LIW-bottom depths, as well as the LIW-layer thickness at the Odas Italia 1 (“W1M3A”) buoy, closely resembles the patterns observed at the Dyfamed observatory, although the pronounced anomaly appears slightly less intense and occurs in 2007.

LIW temperatures and salinities have increased continuously over the past decade at the Odas Italia 1 (“W1M3A”) buoy as in the Dyfamed observatory (Figures 15 and 16) and are in line with the previous cited literature (Schröder et al., 2010; Borghini et al., 2014).



*Figure 13: Vertically averaged salinity above, inside and below the LIW layer (dashed sea green, solid lime green and solid sea green lines in the upper left panel, respectively) at the Dyfamed observatory and their annual anomalies (upper right, lower left and lower right panels, respectively) at the same location. Zero-anomaly values correspond to years in which the annual means equal the climatological means computed over the 1991–2020 period. The grey bands on upper right, lower left and lower right panels are centered on zero and span one standard deviation above and below the climatological means.*



*Figure 14: Depth of the upper and lower boundaries of the LIW layer (“LIW top” and “LIW bottom”) at the Odas Italia 1 (“W1M3A”) buoy (left) and annual anomaly of the LIW layer thickness at the same location (right). Zero-anomaly values correspond to years in which the annual mean equals the climatological mean computed over the 1991–2020 period. The grey band on the right panel is centered on zero and spans one standard deviation above and below the climatological mean.*

### **The composite indicator: the Ligurian Sea Climatic Index**

The Ligurian Sea Climatic Index is then defined as:

$$LSCI(y) = \frac{1}{N} \sum_i \frac{I_i(y) - \bar{I}_i}{\sigma_i},$$

where  $y$  denotes the year, the index  $i$  labels the  $i$ -th component  $I_i$ , while  $\sigma_i$  and  $\bar{I}_i$  are the relative average and standard deviation over the reference period. In words, every component  $I_i$  contributes to LSCI after being properly normalized by subtracting its average and dividing by its standard deviation calculated on the reference period 1991-2020.

Two outcomes are ensured through the normalization procedure: first, all warming and cooling contributions preserve a consistent sign in the final aggregate; second, differences in the absolute magnitudes of the individual components are reduced, allowing each component to contribute more evenly. After normalization and before averaging, anomalies are sign-adjusted based on their correlations with the SST anomaly. Negative signs are thus attributed to the LIW-layer thickness at both the Dyfamed observatory and the Odas Italia 1 (“W1M3A”) buoy.

Figure 17 shows the results of the overall operation, resulting in the composite indicator. Because reanalysis data are available only from 1987 onward, whereas satellite-derived SST observations begin in 1982, the first five years of the LSCI rely only on SST, Thermal Heat Stress, and the MHW-affected Domain Fraction as contributing components.

The LSCI brings together information from multiple physical variables and derived parameters evaluated within the Ligurian Sea domain. The components computed at the three virtual moorings allow relevant processes linked to intermediate and deep waters to be captured effectively. Such processes, together with the associated shifts in temperature and salinity, have been documented throughout the Mediterranean basin over recent decades, particularly after 2005–2006.

The influence of thermal extreme events on ecological systems, especially on habitat-forming species, is also well represented by the LSCI. Although the MHW definition adopted here is purely statistical and relies on climatological percentiles, the index successfully identifies the principal years in which mass-mortality events have been reported in the region (see Estaque et al., 2023). Namely, with the sole exception of 1999, all others years reported in the literature (2003, 2006, 2018, and 2022) appear in the index as marked positive peaks.

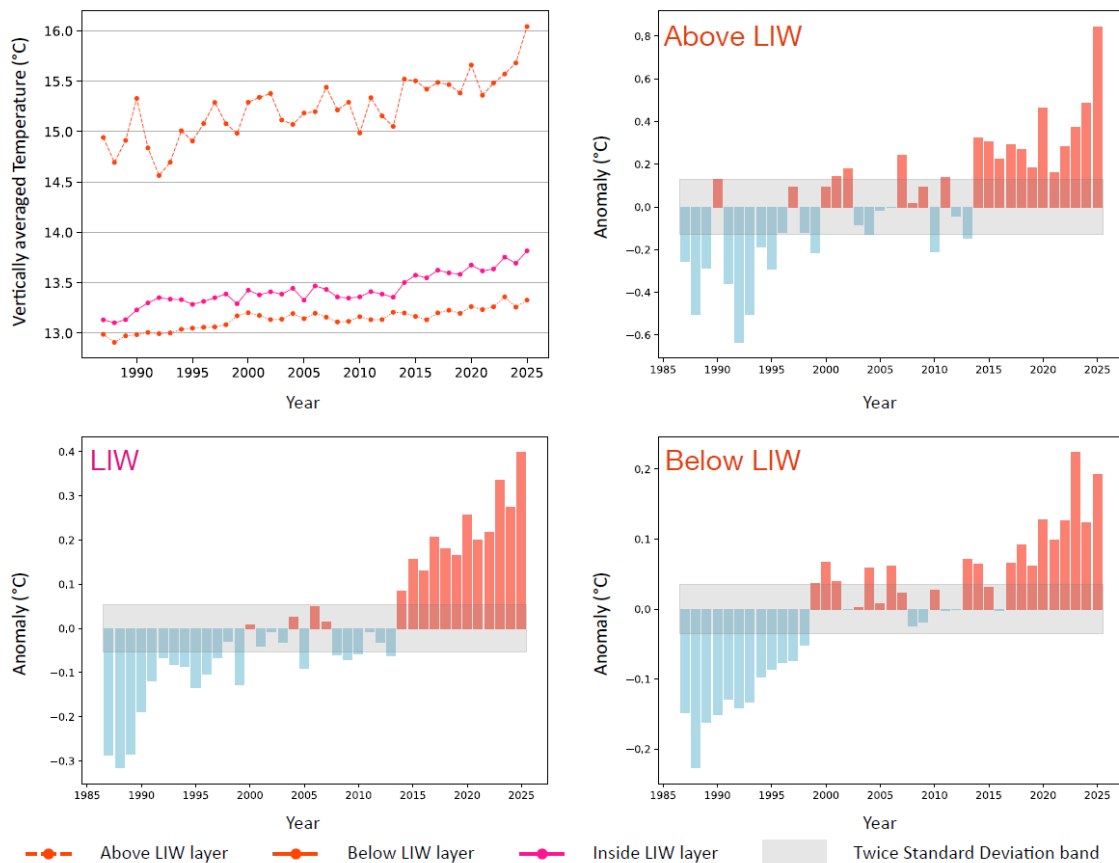


*Figure 15: Vertically averaged in-situ temperature above, inside and below the LIW layer (dashed orange, solid pink and solid orange lines in the upper left panel, respectively) at the Odas Italia 1 (“WIM3A”) buoy and their annual anomalies (upper right, lower left and lower right panels, respectively) at the same location. Zero-anomaly values correspond to years in which the annual means equal the climatological means computed over the 1991–2020 period. The grey bands on upper right, lower left and lower right panels are centered on zero and span one standard deviation above and below the climatological means.*

Overall, the growing trends observed in many of the individual components of the index persist in the composite LSCI, underscoring a growing instability within the Ligurian Sea that is consistent with the larger scale patterns. Without entering the scientific debate surrounding the potential drivers of this dominant behavior, it is evident that the acceleration observed over the past decade is substantial. Moreover, the associated social and ecological consequences, ranging from the increased frequency and intensity of extreme meteo-marine events to the spread of non-indigenous species, are already manifesting in the region.

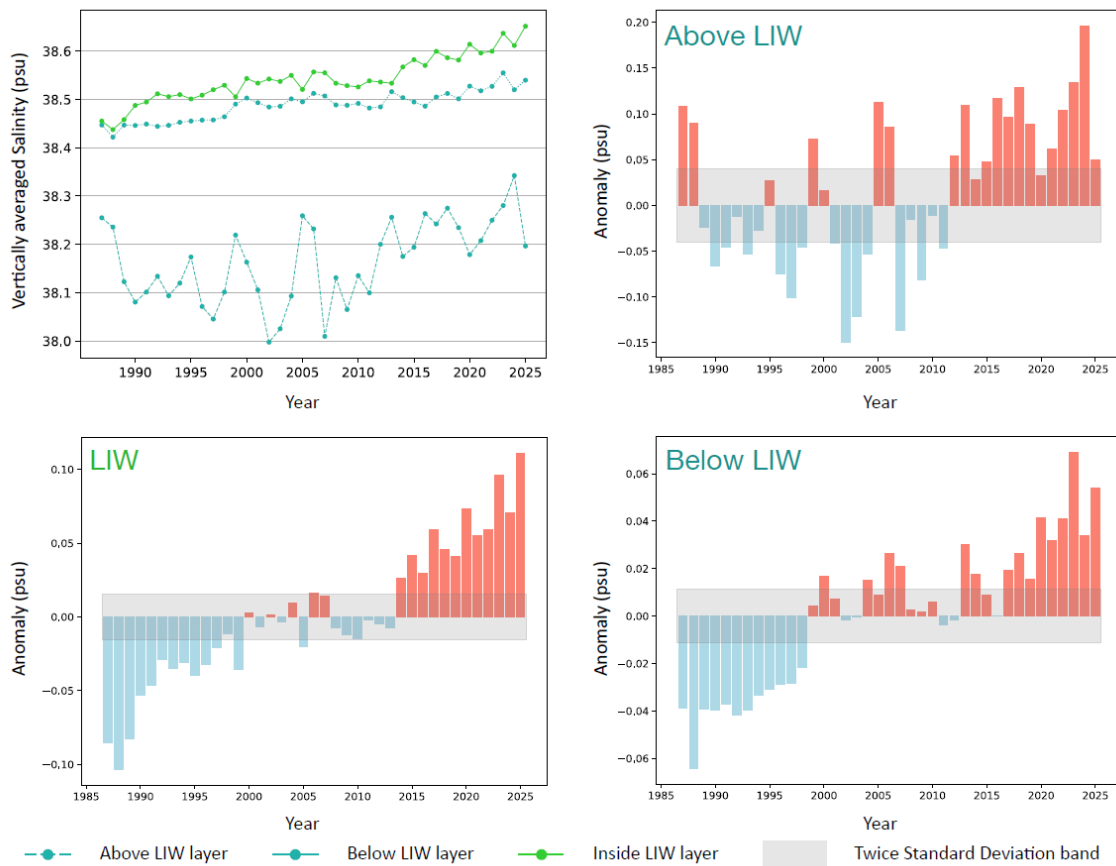


Figure 16: Vertically averaged salinity above, inside and below the LIW layer (dashed sea green, solid lime green and solid sea green lines in the upper left panel, respectively) at the Odas Italia 1 (“WIM3A”) buoy and their annual anomalies (upper right, lower left and lower right panels, respectively) at the same location. Zero-anomaly values correspond to years in which the annual means equal the climatological means computed over the 1991–2020 period. The grey bands on upper right, lower left and lower right panels are centered on zero and span one standard deviation above and below the climatological means.

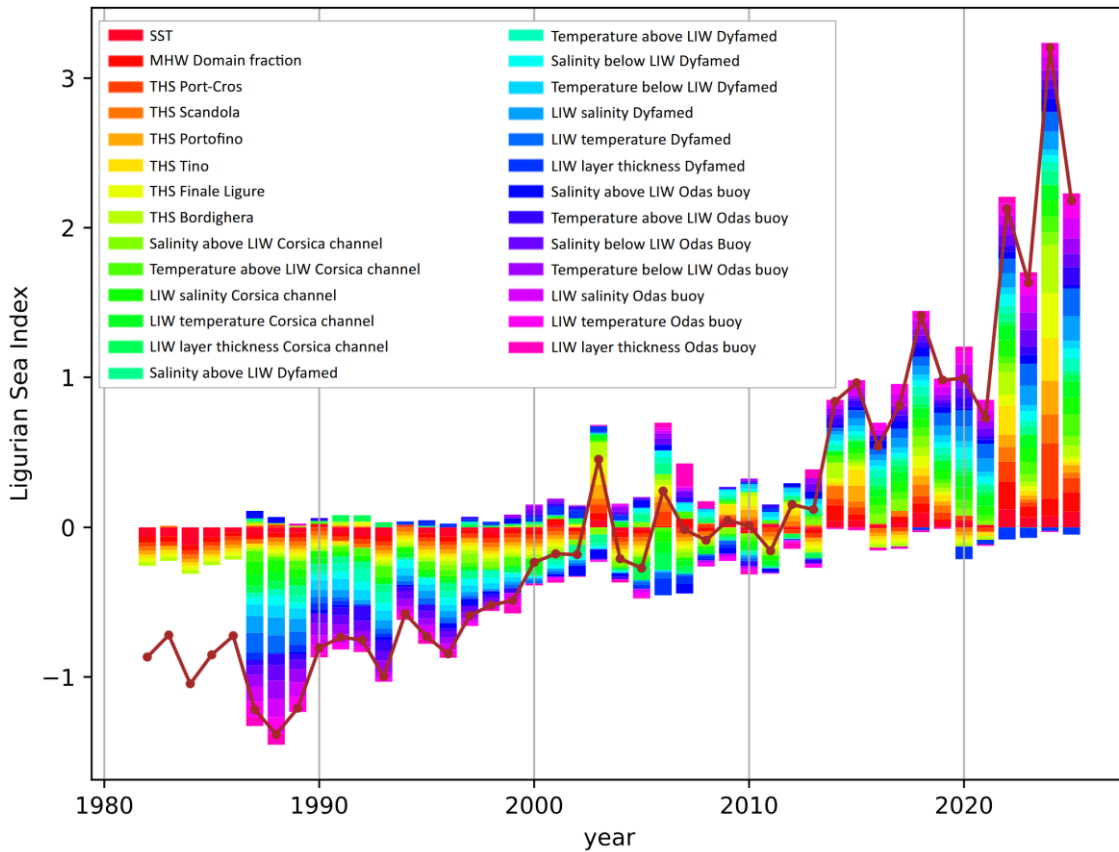


Figure 17: The Ligurian Sea Climatic Index (LSCI). Normalized anomalies from all components are combined and averaged to produce the LSCI (brown line). The height of each colored bar represents the relative contribution of its corresponding component to the overall aggregate. Contributions are computed by dividing each component by the total number of available parameters, including years prior to 1987 when only SST, Thermal Heat Stress, and MHW Domain Fraction were included. This approach ensures a consistent and comparable representation of each component across the entire time series.

### 3. MARINE INVASIVE SPECIES DISTRIBUTION IN CLIMATE CHANGE SCENARIOS

The CLIMA VRE has been employed as part of a Master's Thesis in Environmental Engineering at the University of Genoa. The thesis, authored by the Master's student Marta Falossi and entitled "A machine learning approach for projections of marine species distributions in the Mediterranean Sea under climate change", has been carried out under the supervision of Prof. Andrea Lira-Loarca from the Department of Civil, Chemical and Environmental Engineering and Prof. Annalisa Azzola from the Department of Earth, Environmental and Life Sciences. Given the strong alignment between the topic and the primary objectives of the CLIMA VRE, the main aims, methodological approach, and key results of the thesis work are summarized in this section.

Due to its semi-enclosed configuration, the Mediterranean Sea is particularly vulnerable to climate change and has been identified as a major climate-change "hot spot" (Giorgi, 2006) with an estimated warming trend of about 0.041 °C per year (Kubin et al., 2023). It is undergoing a marked process of tropicalization, driven by warming rates approximately 20% faster than the global average (Lionello and Scarascia, 2018).

Increasing temperatures are fundamentally altering regional biodiversity, favoring the establishment of exotic species of (sub)tropical origin which may push endemic species toward extinction (Bianchi, 2007; Zenetos et al., 2010, 2012). Invasive species are now exceeding 1000 documented taxa and reshaping native food webs and ecosystem dynamics (FAO/GFCM, 2022). *Posidonia oceanica* meadows, one of the Mediterranean's most important carbon sinks, are projected to decline by around 70% by 2050, with potential functional extinction by 2100 (Chefaoui et al., 2018). Some modelling efforts predict global extinction of endemic Mediterranean species (e.g., *Pinna nobilis*, *Patella ferruginea*) by the end of the century (Schultz et al., 2023). Coralligenous assemblages, among the most structurally complex and biodiversity-rich benthic systems in the Mediterranean, are undergoing accelerating degradation as a consequence of increasingly frequent marine heatwaves and temperature extremes (Gómez-Gras et al., 2021). In addition to thermal stress, these habitats are adversely affected by invasive species, nutrient-driven pollution, and sedimentation, all of which diminish structural complexity and disrupt the composition of macroalgal and invertebrate communities (Ballesteros, 2006). Coralligenous frameworks also experience severe physical damage from anthropogenic disturbances, particularly from anchoring (Jimenez et al., 2025).

Forecasting how climate change will alter species distributions is essential because shifting temperatures and ocean conditions are already reshaping habitats and ecological niches. Such forecasts support biodiversity protection by revealing potential ecosystem disruptions before they occur. Ultimately, they enable managers and policymakers to design adaptive strategies that maintain ecosystem resilience under future climate scenarios.

#### **Bio-geophysical climate datasets**

Two types of bio-geophysical datasets have been considered in the work of Falossi (2025) to assess the effects of climate change in the distribution of Mediterranean species. The first type includes both physical and biochemical reanalysis products from the EU Copernicus Marine Data Store. More specifically the potential temperature and salinity fields come from the same Mediterranean Sea Physics Reanalysis dataset (EU-CMEMS 2026b) used in the creation of the Ligurian Sea Climatic Index. The reader is referred to section 2 for a better description of the product. The biochemical variables considered are instead three (pH, chlorophyll concentration and dissolved molecular

oxygen) and come from the Mediterranean Sea Biogeochemistry Reanalysis (EU–CMEMS 2026c). This latter product provides a high-resolution biogeochemical reanalysis of the Mediterranean Sea, offering daily to monthly fields at a horizontal resolution of  $1/24^\circ$  ( $\sim 4$  km) and spanning from 1999 to near-present. It is produced with the MedBFM3 modelling system (Teruzzi et al., 2014), which couples the OGSTM transport model (Lazzari and Bolzon, 2023) with the Biogeochemical Flux Model (BFM, Vichi et al., 2023) and assimilates satellite chlorophyll data through the 3DVAR-BIO scheme (Teruzzi et al., 2018, 2019). The system is forced by the above-cited Mediterranean Sea Physics Reanalysis dataset (EU–CMEMS 2026b) providing the physical fields essential for resolving biophysical interactions. The dataset delivers key ecosystem variables, capturing the structure and functioning of Mediterranean biogeochemistry. The product integrates satellite and in-situ information to generate a consistent reconstruction of biogeochemical dynamics over multiple decades. This comprehensive reanalysis is widely used to study productivity patterns, ecosystem responses to climate variability, eutrophication risks, and habitat conditions for marine resources. Its scientific foundation is documented in Cossarini et al. (2021) demonstrating the value of the MedBFM3 system for high-resolution ecosystem reconstruction across the Mediterranean basin.

As better underlined in the next paragraphs, the two Mediterranean Sea Physics and Biogeochemistry Reanalysis datasets have been used to train the machine-learning model and to establish relationships between the occurrence of invasive species and climatic variables.

The second type of datasets includes bio-geophysical climate projections from the scenarios (see Figure 18) set by the Sixth Assessment Report of the Intergovernmental Panel on Climate Change (IPCC, 2021). These scenarios combine different physical and socio-economic drivers of future climate change by integrating different Representative Concentration Pathways with Shared Socioeconomic Pathways (RCPs with SSPs).

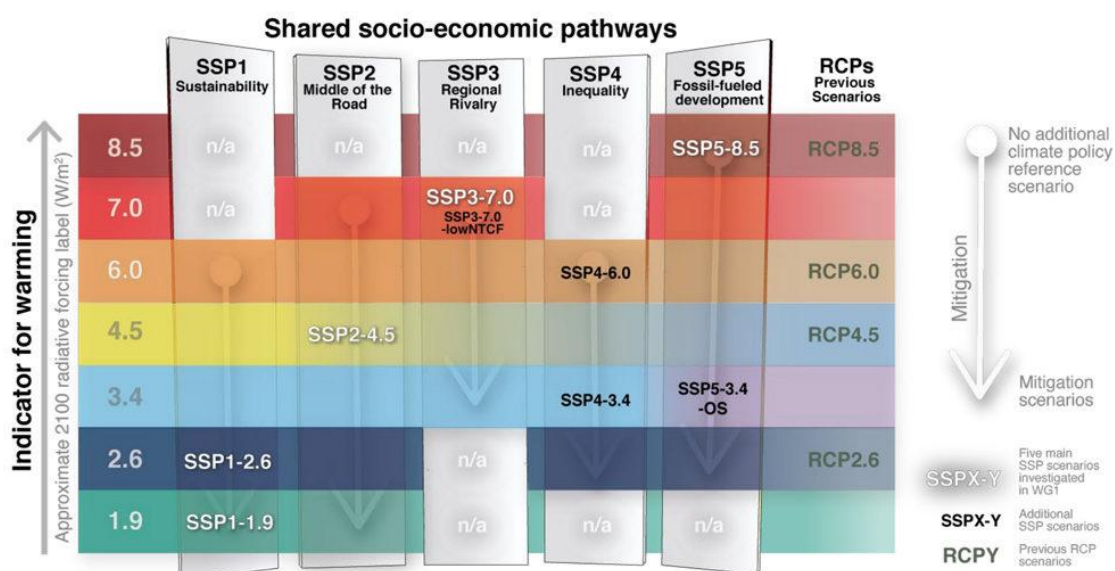


Figure 18: The SSP–radiative forcing matrix as shown in the Cross-Chapter Box 1.4 (Fig. 1) of the Sixth Assessment Report of the Intergovernmental Panel on Climate Change (IPCC, 2021). The SSP socio-economic narratives are shown as columns and the indicative radiative forcing RCP categorization by 2100 as rows.

The RCPs have been introduced to support climate-model experiments and represent distinct trajectories of atmospheric greenhouse-gas concentrations. They are labelled according to their target radiative forcing level expressed in  $W m^{-2}$  in 2100, e.g. RCP1.9, RCP2.6, RCP4.5, RCP7.0 and RCP8.5 stand respectively for target radiative forcing levels in 2100 of +1.9, +2.6, +4.5, +7.0 and +8.5  $W m^{-2}$ . While RCPs allow climate modelers to focus on physical processes, SSPs describe instead plausible evolutions of global society, economies, governance structures, demographics, and technologies through 2100. Each SSP is built as a narrative plus quantitative indicators (population, gross domestic product, urbanization, education). They are namely: sustainable development (SSP1), a “middle-of-the-road” trajectory (SSP2), regional rivalry (SSP3), regional inequality (SSP4) and fossil-fueled development (SSP5). Although developed separately, RCPs and SSPs have been deliberately designed to be cross-compatible: the RCPs describe the climate forcing, while the SSPs describe the world in which that forcing occurs. When combined, they produce a “matrix architecture” (see Figure 18) i.e. a structured set of scenarios that specify both the human systems that shape emissions and the resulting climate responses.

To overcome the coarse spatial resolution ( $\sim 1^\circ$ ) of global Earth-system climate models and to improve robustness of the results, the statistically downscaled projections for the Mediterranean Sea put forth by Kristiansen and Butenschön (2024) have been used. The ensemble product includes downscaled high-resolution ( $\sim 1/12^\circ$ ) simulations for three scenario pathways (SSP1-RCP2.6, SSP2-RCP4.5, and SSP5-RCP8.5) and monthly values for five essential variables (potential temperature, salinity, dissolved oxygen, pH, and chlorophyll) computed at three depth levels (5 m, 25 m, and the seafloor, with chlorophyll restricted to surface waters). The multi-model ensemble is based on five Earth system climate models: CMCC-ESM2 (Lovato et al., 2022), CMCC-CM2-SR5 (Cherchi et al., 2019), GFDL-ESM4 (Dunne et al., 2020), MPI-ESM1-2-LR (Mauritsen et al., 2020) and IPSL-CM6A-LR (Boucher et al., 2020). Bias correction and statistical downscaling is performed using the EU Copernicus Marine Data Store Global Ocean Physics Reanalysis (GLORYS12V1) reanalysis product (EU-CMEMS 2026d), ensuring consistency with observed historical ocean conditions. A detailed description of the statistical downscaling methodology and an evaluation of the resulting datasets across European basins, including the Mediterranean, is provided in Kristiansen et al. (2024).

In the work of Falossi (2025), two downscaled scenarios of the above matrix have been selected:

- the “intermediate” scenario SSP2-RCP4.5 (better indicated with the shorter and more common version SSP2-4.5), i.e. a “middle-of-the-road” pathway and a moderate mitigation and partially effective climate policies;
- the worst-case scenario SSP5-RCP8.5 (better indicated with the shorter and more common version SSP5-8.5), i.e. a “business-as-usual” pathway driven by fossil-fuel development, rapid economic growth, and weak or absent climate policies.

The above climate projections have been used after the model training phase, to assess future patterns in the spread of alien species.

### **Biological datasets**

For large parts of the Mediterranean Sea, biological observations are still very limited (Levin et al., 2014). After an extensive literature review process, Falossi (2025) has selected, organized and standardized the following three sources for biological datasets which provide verified, geo-referenced records reporting at least the observation year: Azzurro et al. (2022a, 2022b), Katsanevakis et al. (2020) and Ragkousis et al. (2023).

To prepare the biological records for use in a machine-learning framework, data from the above three independent sources have been harmonized into a single structured dataset. Because one of the datasets (ORMEF, Azzurro et al. 2022a) only reports observations at the annual scale, the temporal resolution of the entire dataset has been set to the yearly level. The variables selected for the analysis are then species name, year of observation, and geographic coordinates.

The final merged dataset contains 21704 standardized records and serves as the foundation for the machine-learning analyses presented in the following sections.

### **The machine learning model**

The construction of a machine-learning model to predict future distributions of marine alien species in the Mediterranean Sea has represented the key methodological component of the work by Falossi (2025). The modelling pipeline has been designed as a sequence of well-defined steps, from data preprocessing to model training (fitting) and validation (Figure 19).

To predict future occurrences, the model must first learn the statistical relationship between historical species observations and the environmental conditions present at the same time and location. Once this relationship has been established through training and validation, it can be applied to climate-projection datasets to estimate the probability that a given location will be suitable for alien species in the future.

To facilitate spatial comparisons, the output of the model has been casted as “suitability index”, i.e. the probability that a grid cell will contain at least one alien species in a given year. This formulation naturally leads to a binary classification problem, where each grid cell is assigned a positive (presence) or negative label (absence). However, biological observations provide presence-only information as locations without alien-species records cannot be treated as “true absences”, because sampling effort is uneven across space and time. The modelling framework has then incorporated a “pseudo-absence” generation algorithm (“background selection” function) by randomly labeling a 10% subset of unsampled grid cells as pseudo-absence points. This approach is common in species-distribution modelling when true absence data are unavailable (e.g. Barbet-Massin et al., 2012).

Parallel to this procedure, climate data have been transformed using a Maximum Entropy (MaxEnt) approach, i.e. through the MaxEnt-style feature builder described in Phillips et al. (2006). The builder generates derived predictors (linear, quadratic, hinge) to capture potentially complex relationships between environmental predictors and species presence.

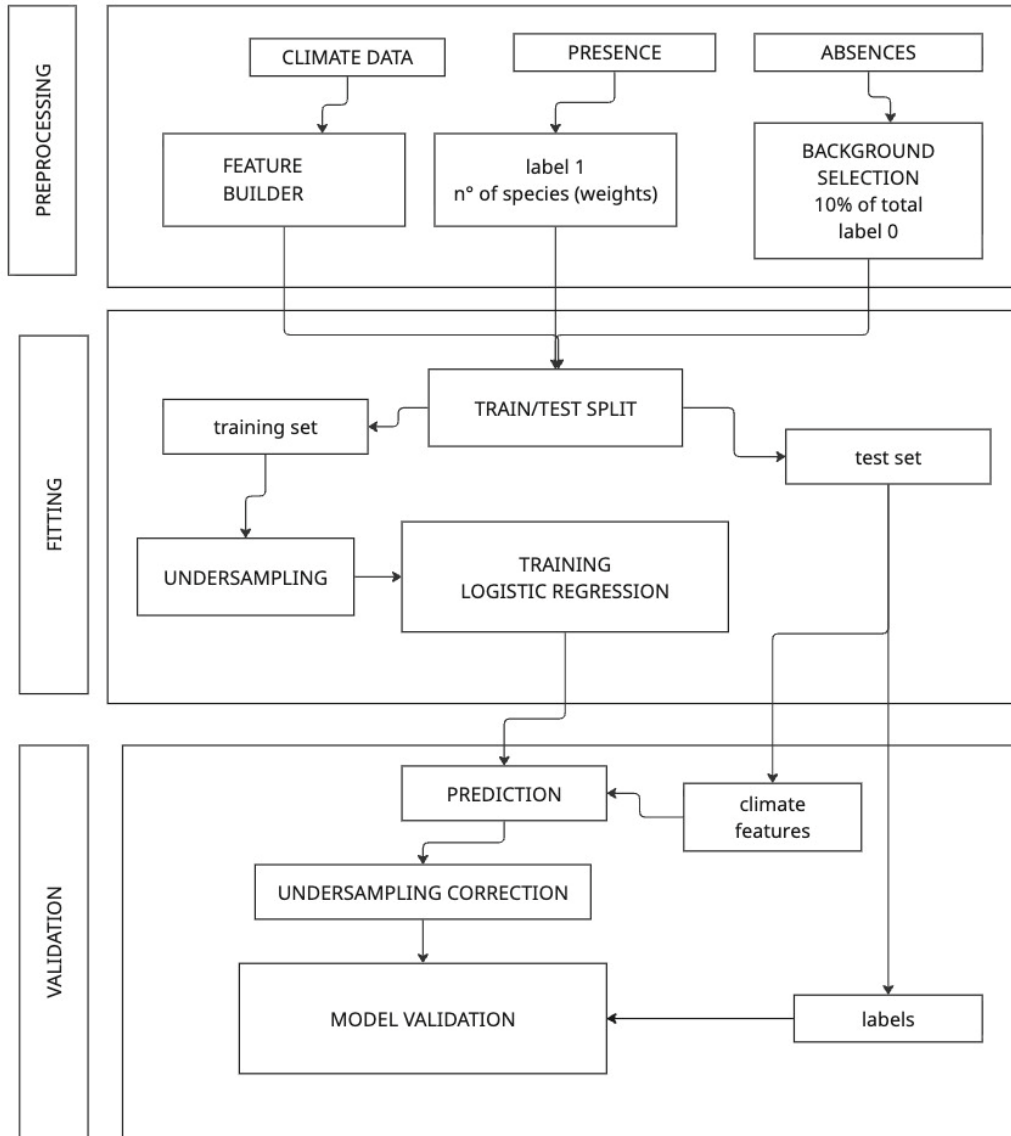


Figure 19: Descriptive scheme of the machine learning model used in Falossi (2025).

Following the preprocessing step, an input dataset has been constructed in which each grid cell contains the transformed environmental predictors, a binary presence/pseudo-absence indicator, and the number of distinct alien species recorded at that location. This last variable is retained as a “weight” parameter, meaning that grid cells with observations of multiple alien species contribute proportionally more to the model during training.

Because observations before 2010 are too sparse to support reliable modelling, the input dataset has been restricted to the 2010–2021 period. The resulting dataset consists of 4949 presence records and 178466 pseudo-absence points. Presences are then only about 2.7% of the total dataset, highlighting the severe imbalance between positive and negative instances. This imbalance has the following two important repercussions: a) on the choice of logistic regression, i.e. a class of models whose algorithms are stable, interpretable, and suited to imbalanced binary classification; b) on the need of an undersampling strategy thanks to which all presences have been retained, while an equal number of pseudo-absences was randomly selected to create a balanced training set. This approach improves the algorithm's ability to learn from the minority class but artificially alters class proportions. Predicted probabilities must be then corrected after training.

Four logistic-regression models have been evaluated. They differed in predictor sets (physical only vs. physical plus biogeochemical variables), weighting schemes (presence counts as sample weights), and validation strategy (train–test split vs. five-fold cross-validation). Because traditional metrics such as accuracy are misleading under severe imbalance, model performance has been assessed using precision and recall for the positive class. Recall is especially important for ecological applications, as failing to detect true presences (false negatives) is more detrimental than generating false positives.

In Falossi (2025) the best model has resulted to be the one combining all predictors with sample weights and cross-validation since it has achieved the best trade-off, with a recall of 0.416. Although precision has been modestly lower than for the other simpler models, this configuration has maximized the model's ability to detect potential invasion hotspots, aligning with ecological monitoring and management priorities.

The paragraphs below report exclusively the results produced by this best model.

### **Suitability maps**

Falossi (2025) analysis of the results has been carried out in many directions. Here only some thesis outcomes are described to showcase the use of the CLIMA VRE with a focus mainly on suitability maps for the historical period and for future projections. The reader is referred to the Falossi (2025) thesis for a comprehensive and detailed analysis of all results including a specific application in the Sicilian area.

Figure 20 illustrates the best model output for selected historical years: the colorscale indicates the predicted Suitability Index, while blue points mark the observed alien-species records used during training. Overall, areas with high predicted suitability correspond well to known presence locations, confirming that the model successfully captures the main spatial patterns of alien-species occurrence. Nonetheless, some regions show persistent mismatches. Along the Egyptian coast, for example, suitability values are consistently high despite the absence of reported observations. Given the region's proximity to the Suez Canal, its warm thermal regime, and the abundance of invasion records in neighboring countries, this mismatch is likely a consequence of limited or uneven monitoring rather than a true absence of alien species.

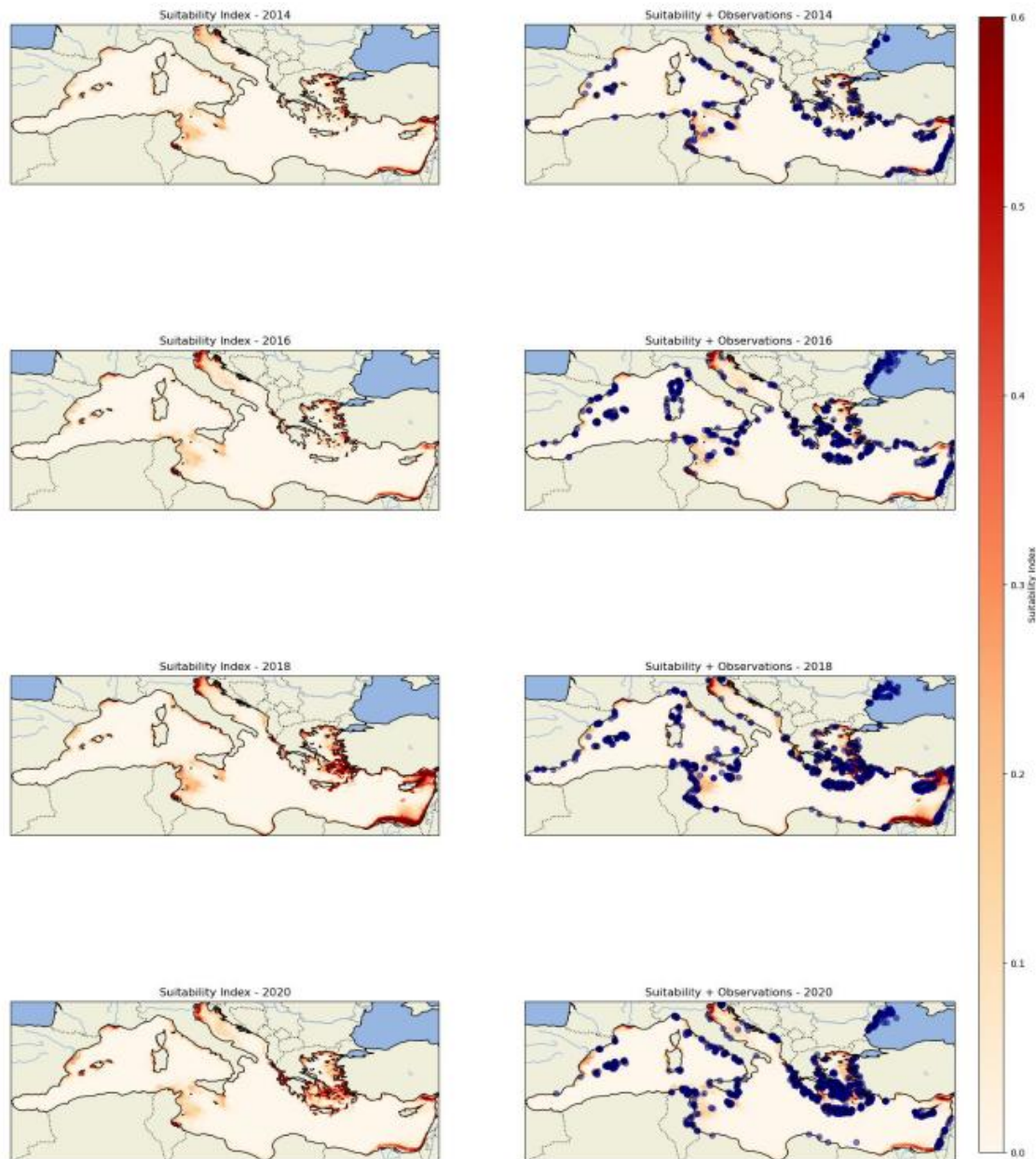


*Figure 20: Comparison between suitability index from the best model and real observations (blue dots) in different years, namely 2014, 2016, 2018 and 2020 as shown in Falossi (2025).*

A different situation appears along the southern French coastline, where high suitability does not coincide with frequent alien-species detections. This may indicate that factors unrelated to climate, such as local ecological resistance, habitat characteristics, or anthropogenic pressures, limit alien settling despite favorable environmental conditions. Such areas warrant further ecological investigation.

Overall, these results show that the model effectively identifies zones of high invasion risk and mirrors the distribution of known presences, while also highlighting locations where observation gaps or ecological dynamics may explain discrepancies. This reinforces the model's utility both for interpreting past invasion patterns and for informing current management policies.

The analysis of the suitability maps for the future projections has considered the following time periods:

- Near-future period: 2025–2035;
- Mid-century period: 2050–2060;
- End-century period: 2085–2095.

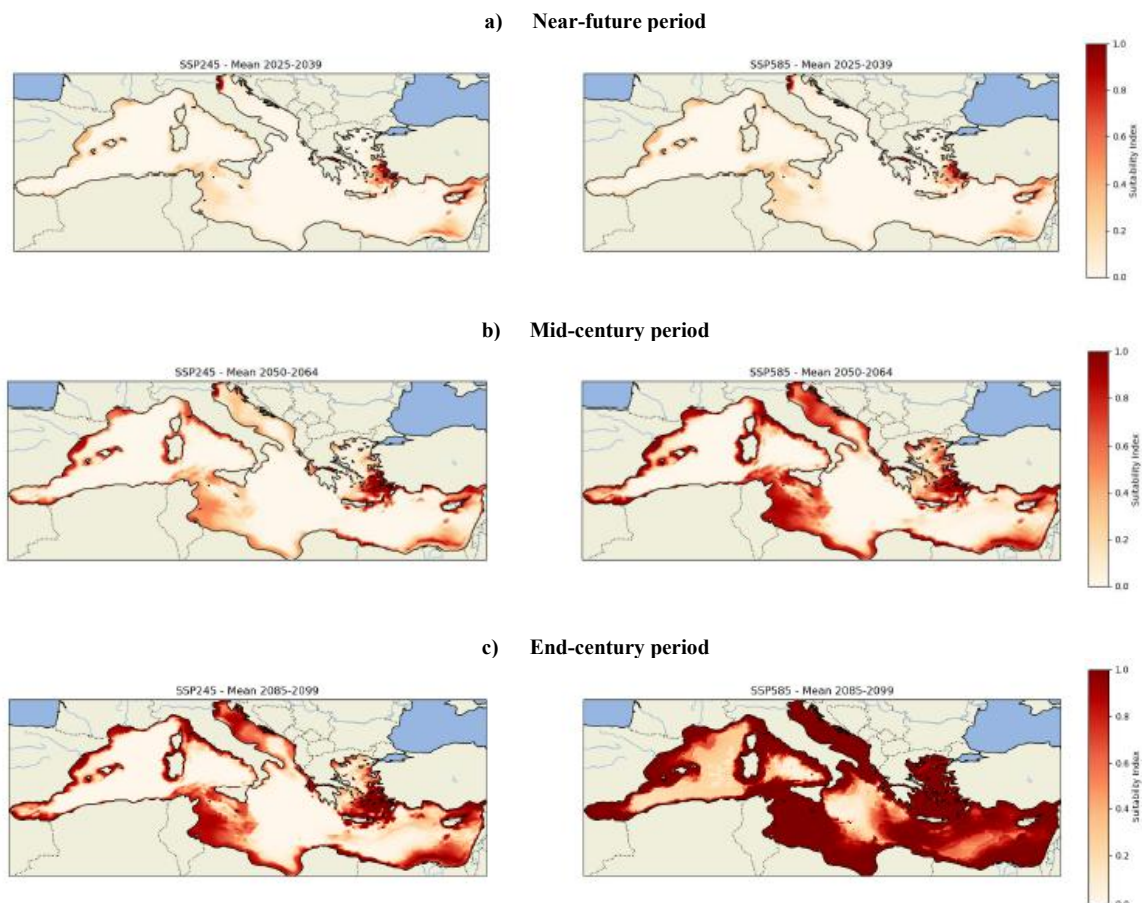


*Figure 21: Averaged suitability index for the SSP2-4.5 (left panels) and SSP5-8.5 (right panels) scenarios. Upper, middle and lower panels show the Falossi's (2025) results for the a) near-future, b) mid-century and c) end-century periods, respectively.*

Figure 21 shows averaged suitability maps over each of the above periods produced for both SSP2-4.5 and SSP5-8.5 scenarios. The two scenarios display similar trends in the near-future period but begin to diverge significantly by mid-century and end-century. Under SSP5-8.5, suitability values are markedly higher, particularly along the Tunisian coast, southern Sicily, and the eastern Italian coastline. A larger extent of the suitability area is predicted by the model in the SSP5-8.5 scenario and by the end of the century: extending potential habitats can be found even into offshore areas far from the coast. Although uncertainty inevitably increases with time, the trend remains consistent. In both scenarios, a clear increasing trend is observed, indicating that areas suitable for alien species invasions are expected to expand in the coming decades. This highlights the urgent need for strengthened prevention and management strategies to ensure biosecurity and mitigate the risk of irreversible damage to existing ecosystems.

#### 4. OTHER APPLICATIONS OF THE CLIMA VRE

In this section two other applications of the CLIMA VRE are introduced. They highlight the remarkable flexibility of Virtual Research Environments, illustrating their ability to address research challenges and applications that lie outside their original scope.

##### **Marine connectivity studies in Tanzania**

The CLIMA VRE has been also used analysis of coral reef connectivity along the Tanzanian coastline aimed at identifying Marine Protected Areas (MPAs). Part of this study represents the Master's Thesis in Environmental Engineering at the University of Genoa authored by the Master's student Andrea Valli and entitled "Dispersal processes and connectivity studies in the marine environment for the realisation of Marine Protected Areas in Tanzania". The thesis work has been carried out under the supervision of Drs. Marcello Magaldi, Roberta Sciascia and Michele Bendoni (CNR-ISMAR-Lerici) and Prof. Giovanni Besio (Department of Civil, Chemical and Environmental Engineering of the University of Genoa). The main aims, methodological approach, and key results of the work are summarized in the next paragraphs.

The study region includes the mainland coasts of Tanzania, Mafia Island, Zanzibar Island, Pemba Island. Surface current velocities from the Western INdian ocean Simulation model (WINDS, Vogt-Vincent and Johnson, 2022) have been utilized to conduct a Lagrangian dispersion experiments using the Ocean Parcels tracking simulator (Delandmeter and Van Sebille, 2019). The focus of this study has been on two coral taxa: *Acropora* and *Porites*, selected due to their ecological significance and their differing biological traits. Surface current data from different years, specifically 1997, 1998, and 1999, have been selected to analyze inter-annual variability in connectivity. The Ocean Parcels simulator has been implemented to spread particles during specific periods of the year to represent coral larvae spawning behavior. The analysis of connectivity matrices for various seasons and years has allowed to identify critical coral reef sites that are essential to the ecosystem and require protection.

Marine biodiversity is declining mainly due to human pressures such as overfishing and coastal development, with destructive practices like bottom trawling severely damaging habitats such as coral reefs. Marine Protected Areas (MPAs) have become essential tools to counter these impacts (Mellin et al. 2016), evolving into interconnected networks that enhance ecological connectivity and support species movement and ecosystem resilience. Connectivity between MPAs enables the exchange of individuals and genes, improving recovery after disturbances and helping ecosystems adapt to environmental change (Almany et al. 2009).

For corals, larval connectivity depends on both oceanographic conditions (e.g., currents) and biological traits (e.g., spawning times, competency periods, settlement behavior), with dispersal ranging from meters to hundreds of kilometres (Gawarkiewicz et al. 2009; Domingues et al. 2012). Quantifying larval movement is crucial for identifying recruitment sources and designing effective MPAs, yet research is challenging because biological parameters are often derived from laboratory studies and model reliability decreases at larger spatial and temporal scales. To address this, advanced models integrate hydrodynamic simulations with biological data, and particle-tracking techniques allow researchers to map dispersal pathways, identify source–sink dynamics, and improve predictions by combining laboratory knowledge with field observations.

The Western Indian Ocean Simulation (WINDS, Vogt-Vincent and Johnson, 2022) is a regional configuration of the Coastal and Regional Ocean Community Model (CROCO, Auclair et al. 2025) specifically designed for the southwestern Indian Ocean. WINDS has a horizontal resolution of approximately 2 km and spans from 23.5 °S to 0 °N in latitude and from the East African coast to 77.5 °E in longitude. Two experiments have been conducted using the WINDS configuration: WINDS-M, a full 28-year multidecadal simulation (1993–2020), and WINDS-C, a 10-year climatological control run with monthly climatological forcing. Horizontal surface velocities are recorded every 30 minutes, while other surface fields are available as daily output. Additionally, the complete 3D temperature, salinity, and velocity fields are available every 5 days. WINDS effectively reproduces surface temperature, salinity, currents, and tides in the southwestern Indian Ocean, making it suitable for regional marine dispersal studies involving buoyant particles or other applications requiring high-resolution surface ocean properties.

Ocean Parcels (Delandmeter and Van Sebille, 2019) is a Python-based framework designed to create customizable particle tracking simulations using output from ocean circulation models. It is primarily written in Python, incorporating low-level C code and just-in-time compilation for efficient computation. It enables the tracking of both passive and active particulates, including water, plankton, plastic, and fish. The foundation of Ocean Parcels particle tracking lies in the particle tracking equation proposed by Lange and van Sebille (2017):

$$\vec{X}(t + \Delta t) = \vec{X}(t) + \int_t^{t+\Delta t} \vec{v}(\vec{x}, \tau) d\tau + \Delta\vec{X}_b(t) ,$$

where  $\vec{X}(t)$  represents the particle's position at time  $t$ ,  $\vec{v}(\vec{x}, \tau)$  is the ocean velocity field (in this case provided by WINDS), and  $\Delta\vec{X}_b(t)$  denotes the change in position due to various effects, such as random motion. The Runge-Kutta 4 method has been used for a better balance of performance with computational effort, relative to the accuracy and consistency of the method. A linear interpolation has been applied to approximate the ocean velocity field at locations where it is not explicitly defined on the WINDS grid.

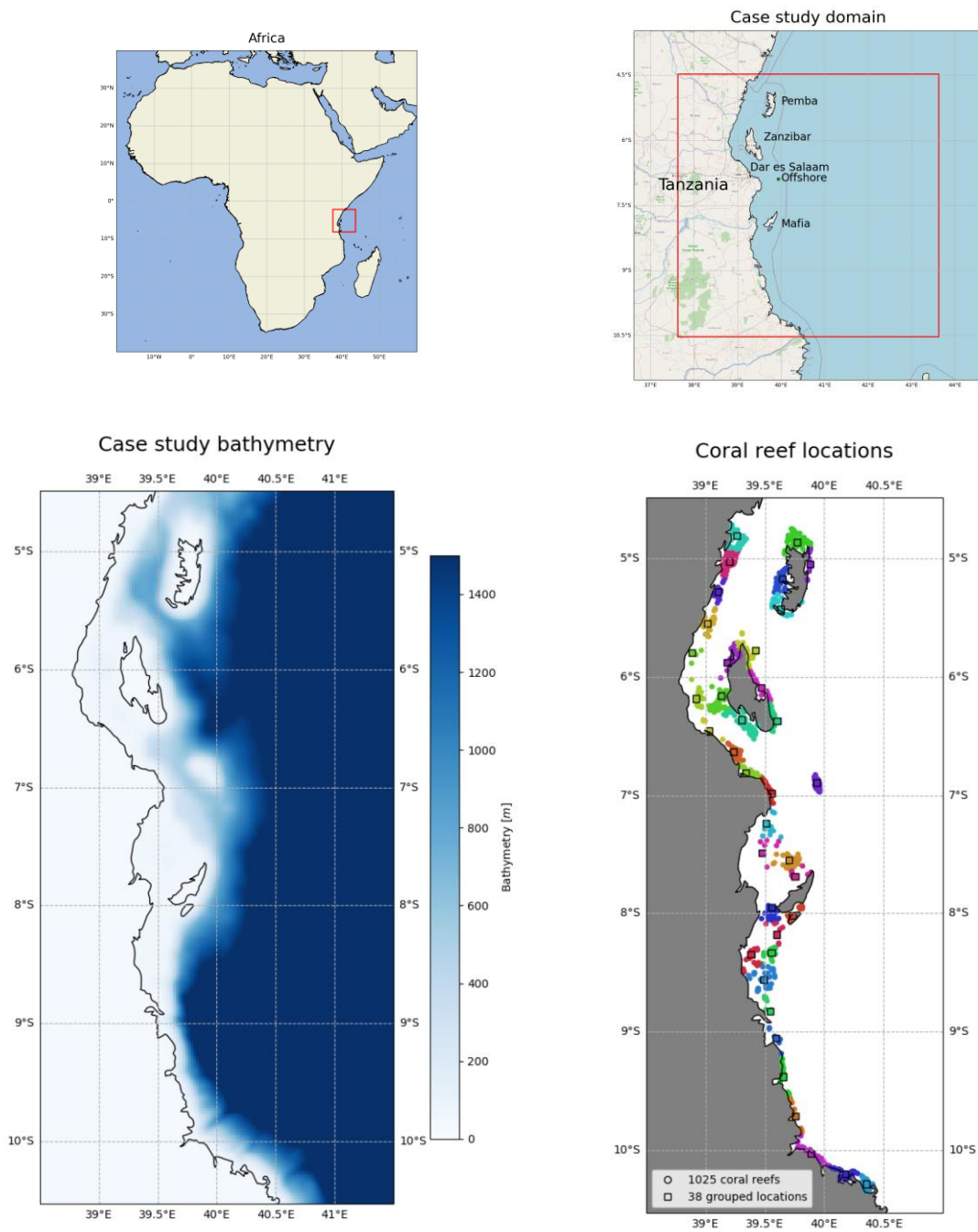


Figure 22: Upper panels: simulated domain and position in the African continent. Lower panels: bathymetry of the numerical domain (left) and locations of the coral reefs (right). Black-contoured squares represent 38 aggregated coral reef groups. Circles represent the sampled reefs highlighted and color-coded to indicate their respective reef groups.

The simulated domain covers the coasts of Tanzania from 37.62 °E to 43.62 °E and from 4.47 °S to 10.52 °S (Figure 22). Three are the main islands included in the domain, namely Pemba, Unguja and Mafia. The bathymetry in the domain is very diverse with the offshore deeper parts exceeding depths of 2000 m and the coastal shallower regions having characteristic depths of a few tens of meters. Noteworthy is the Pemba Channel (39.3 °E, 5.2 °S), which separates the island of Pemba from the East African mainland with relatively deep waters with maximum depths at about 800 m.

Historical coral reef studies in Tanzania began in 1965 and were initially sparse, descriptive, and geographically limited, though they informed early management and MPA planning. The most comprehensive assessment for Pemba Island (Grimsditch et al. 2009) reported strong spatial variability in reef condition, with average hard coral cover at 23% but ranging from 86% in protected Misali to only 3–5% in heavily degraded sites. Healthier reefs were dominated by hard corals, while degraded areas were overgrown by rubble and turf algae. Surveys from the 1980s–1990s showed widespread degradation driven by overfishing and destructive practices such as dynamite fishing. Although dynamite use declined, subsequent assessments in 1999–2000 showed further coral loss linked to the 1998 mass-bleaching event, with mortality patterns varying by location and species. Despite substantial bleaching impacts, some reef structure remained intact and early signs of recovery, through surviving colonies and new recruits, were observed.

Coral bleaching occurs when stress, primarily elevated sea temperatures, breaks down the symbiosis between corals and their algal partners, leaving the white skeleton exposed. Events are most severe during warm anomalies such as El Niño, though cold shocks, high solar radiation, and pollution can also cause localized bleaching. Tanzanian reefs have been heavily impacted, especially during the 1997–1998 global bleaching event, when temperatures rose ~2°C above normal and caused up to 80–90% mortality in places like Misali and Tutia (Muhando and Mohammed, 2002). Many reefs showed limited recovery because prolonged bleaching starved corals of their algal food source. A later event in 2016 was milder, with Zanzibar reefs largely recovering. Around Pemba, coral cover dropped from 54% to 12% after 1998 and only partially rebounded to 16% by 2002 (Obura et al. 2002). Strengthening reef protection, expanding MPAs, and supporting restoration and monitoring programs are thus essential to improve long-term reef resilience.

*Acropora* and *Porites* corals along the Tanzanian and wider Western Indian Ocean coastline exhibit complex reproductive patterns, connectivity, and responses to environmental stress. *Acropora* species show extended and weakly synchronized spawning seasons, with gamete release occurring from October to April (Mangubhai and Harrison, 2006) and peak reproduction between January and March, indicating temporal reproductive isolation and diverse lunar-temperature cues. Some species, such as *A. tenuis*, maintain nearly continuous gametogenic cycles. Large-scale genetic analyses demonstrate high connectivity of *A. tenuis* across East Africa (van der Ven et al., 2022), supported by long Pelagic Larval Duration (PLD) and northward transport via the East African Coastal Current, though localized genetic structuring still occurs.

*Porites* species, including the widespread *P. lutea*, rely mainly on broadcast spawning and exhibit connectivity patterns that vary with oceanographic conditions, as shown in a Seychelles-focused dispersal modeling effort (Burt et al., 2024). Larval behavior also shapes population structure: *P. lobata*, with a PLD of ~30 days, has more limited dispersal potential compared to *Acropora*. Together, these reproductive traits and connectivity patterns influence each genus's resilience, capacity for recolonization, and response to disturbances in Western Indian Ocean reef systems (Randall et al., 2024).

The coral reef locations that has been used in this study come from high-resolution Benthic Ecological Surveys conducted by the Wildlife Conservation Society along the Tanzanian coast. Field-based coral cover measurements, although spatially limited, are more accurate than satellite-derived estimates, which often misclassify reef areas due to depth, turbidity, and structural complexity (Hedley et al 2016; Lyons et al 2020). Satellite products used in prior work consistently overestimated coral cover compared with in-situ observations (Vogt-Vincent et al. 2023). From the 1137 points surveyed by the Wildlife Conservation Society and containing hard corals, land-based points inside the WINDS model domain have been removed using a velocity-mask filter, yielding 1025 valid oceanic reef sites for particle-tracking simulations. This study has adopted a strategy similar to previous works (e.g. Vogt-Vincent et al. 2023) that grouped reef sites into several clusters to simplify connectivity analyses. The resulting dataset contains 38 reef groups, which serve as the spatial units for evaluating larval connectivity (Figure 22, bottom left panel).

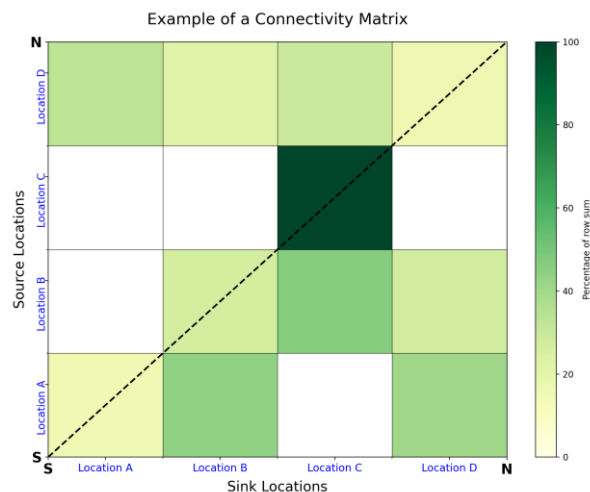


Figure 23: Illustration of a 4x4 connectivity matrix with locations arranged from South to North.

Connectivity matrices describe how coral reef sites exchange larvae, providing a quantitative framework to understand linkages within a reef network. They are essential tools for designing MPAs, helping identify key source and sink reefs that sustain regional biodiversity and ecological resilience. The matrices also support conservation planning by highlighting sites with strong larval exchange and informing predictions of population responses to environmental change. Each matrix element represents the probability or strength of larval movement between two sites, based on data from oceanographic models, genetics, or tracking studies. In the example 4x4 matrix shown in Figure 23, rows denote larval sources and columns denote sinks, with the diagonal indicating self-recruitment. The lower-right triangle reflects south-to-north connections, while the upper-left shows north-to-south dispersal. Because each row sums to 100%, it captures the full fate of larvae released from a given site, whereas column totals indicate the relative importance of each site as a larval sink.

Two months, April and November, have been selected to represent the spawning period for both *Acropora* and *Porites* taxa as their spawning period extends from October/November to March/April. The study has aimed at comparing the hydrodynamic and connectivity associated with the years 1997, 1998, and 1999 as they represent the year before, during and after the important bleaching 1998 event. The Pelagic Larval Durations (PLDs) for *Acropora* and *Porites* have been set to 70 and 30 days, respectively. Connectivity matrices have been generated for each period and taxa. The analysis has started by selecting 1025 reef locations within the model domain, each represented by a  $0.02^\circ \times 0.02^\circ$  cell. Within every cell, nine additional random release positions have been generated, yielding a total of 10250 particle release points. Particles have been released hourly between 18:00 and 05:00 over the course of one month and advected using surface velocities for a period matching the PLD, i.e. 70 days for *Acropora* and 30 days for *Porites*. After these periods, each particle's final position has been assessed: if it lays within  $0.02^\circ$  of any of the 1025 original locations, it has been considered to have reached that site.

If a particle arrives within the proximity of one of the 38 aggregated reef groups, it has been assigned to the nearest group. Similarly, the particle's starting point has been mapped to the nearest of the 38 groups to ensure a consistent square connectivity matrix. This procedure has produced a  $38 \times 38$  connectivity matrix, representing source–sink relationships, for each of the two taxa and PLD scenarios. The entire workflow has been repeated for November 1997 and for the subsequent years 1998 and 1999 to capture interannual variability.

Connectivity matrices have been computed spanning the parameter space for two taxa (*Acropora* and *Porites*), three years (1997, 1998 and 1999) and the spawning events taking place during two months (April and November). Each connectivity matrix features the grouped source locations on the y-axis, representing where the coral larvae start during the spawning event. The x-axis lists the same grouped locations as sink spots, indicating where the coral larvae end their trajectories based on their PLD. These spots are arranged from the southern to the northern positions. The strongest values often lie in the diagonal connections because of local currents that prevent larvae from spreading beyond these small areas. It is important to highlight that no particle can re-enter the domain once exited as particle trajectories are deleted once they reach the boundary of the simulated domain. A particular care is also taken in handling boundary conditions near material boundaries (i.e. near land points) to ensure accurate and realistic particle trajectories. If moved towards land, a particle will continue to stay in a cell close to a material boundary until the velocity changes direction and moves it away from the land to offshore areas.

Figure 24 shows how ocean currents influence particle trajectories in the months of April and November 1999. Each particle is color-coded in the Figure based on its cluster group, allowing for easy visual tracking of group-specific movement patterns. Almost all particles are advected northward, consistently with the presence of the East African Coastal Current. During the first 10 days of April however, particles are advected northward more intensely due to the stronger current moving along the eastern side of Pemba Island and only a few travel to the western side, while in November, they tend to stay closer to the coast.

Many connectivity matrices have been calculated in the study. Here only some matrices are described to showcase the use of the CLIMA VRE while the reader is referred to the Valli (2024) thesis for a comprehensive and detailed analysis of the results. Figure 25 compares the connectivity matrices at 30 days post-release between April and November in the year 1997 and 1999. The locations are arranged from the southernmost to the northernmost and grouped in 38 major reef clusters (Figure 22). The dashed colored lines in the connectivity matrices outline the cells surrounding the three islands, whereas solid colored lines highlight self-recruitment. The “Offshore” spot, corresponds to

Latham Island a small 3-hectare island. The color bar represents the percentage of the sum of the rows' values.

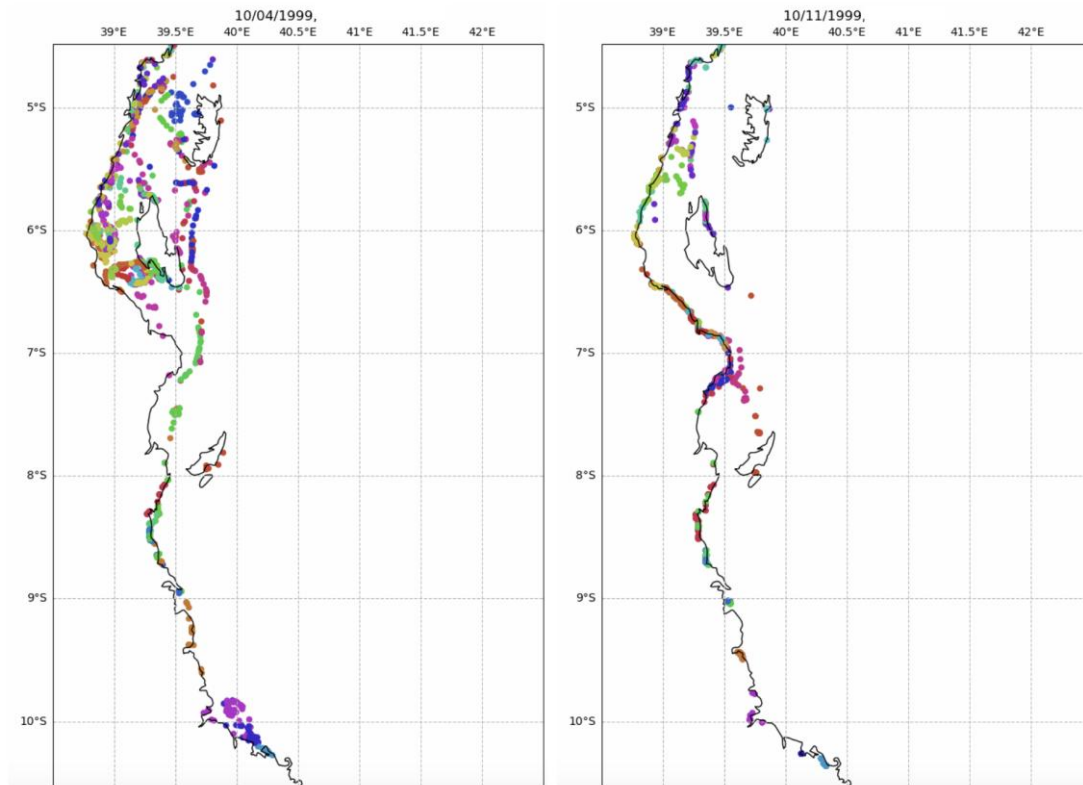
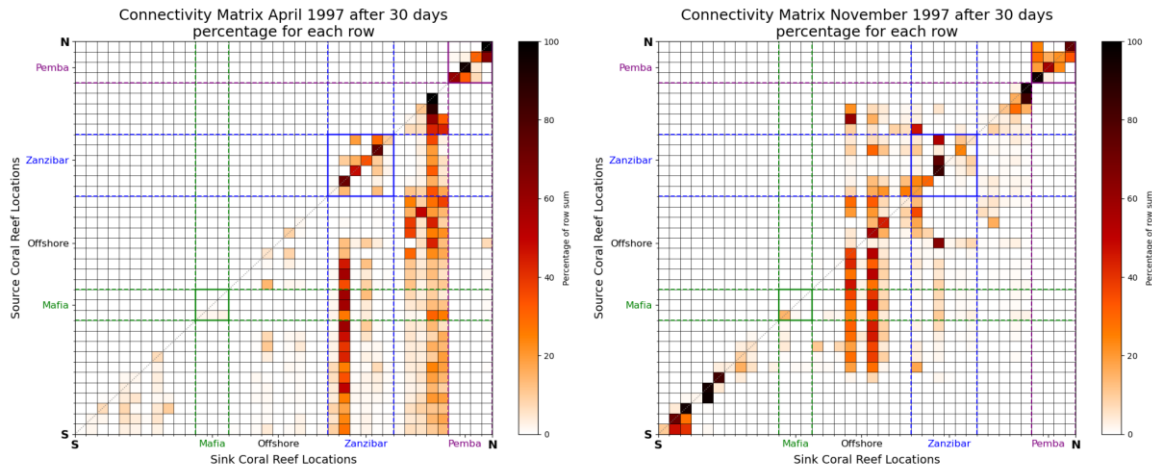


Figure 24: Comparison of particle trajectories in April and November 1999. Each particle is color-coded based on its cluster group.

In April 1997 (upper left panel), a few locations are connected to the southward locations, as shown by the largely empty upper-left triangle. In contrast, during November 1997 (upper right panel), several southward connections are present, although they are smaller in intensity. Specifically, there are more connections between spots near Mafia Island and reefs along the mainland coast around Dar es Salaam in November compared to April. A notable observation is that Pemba Island (purple square) is only connected with itself as a sink location in both matrices. Furthermore, both matrices illustrate that coral larvae originating from the east coast of Pemba Island cannot reach the west coast, and vice versa. In 1999 (lower panels) the overall characteristics of the matrices remain similar to those of 1997, with notable exceptions. One exception is the almost complete absence of north-south connections in November. Another one is the Offshore spot, which is connected to the southeast part of Pemba, but only during April. In April 1999 however, there are no connections among the reefs below Zanzibar Island, except for the spot located on the southern side of Mafia Island, which exhibits some self-recruitment.

a) 1997



b) 1999

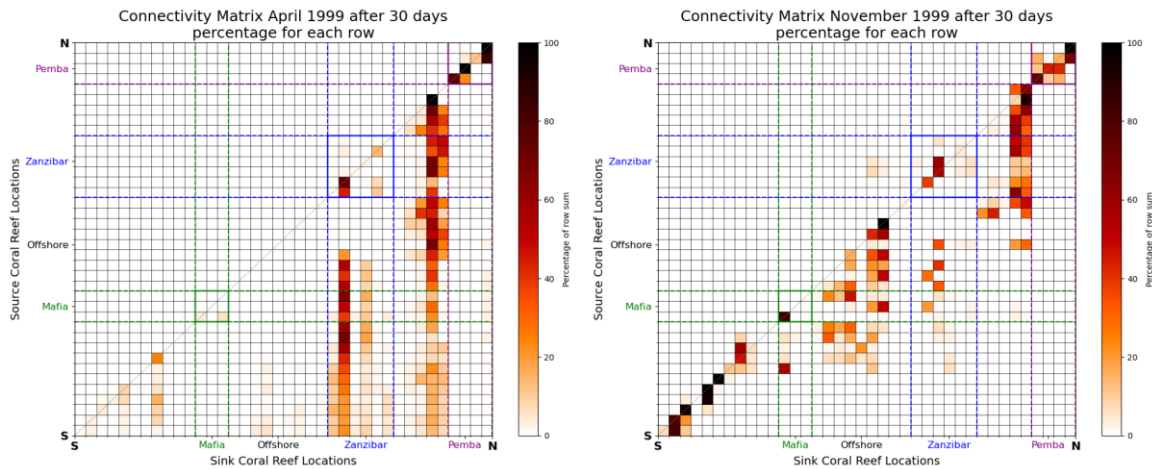


Figure 25: Connectivity matrices at 30-days post-release for years 1997 (upper panels) and 1999 (lower panels). Left and right panels show results in the months of April and November, respectively.

For all years, the locations along the southern coast of Tanzania show high retention rates in November, conversely in April they are connected with the northern part of the coast, especially Zanzibar. Due to the prevailing currents, across all these figures, the northernmost spots are exclusively interconnected among themselves.

At 70 days post-release (not shown), November connectivity matrices show broader, more symmetrical links, especially from Latham Island to Zanzibar, while April closely resembles earlier patterns with similar connection strengths. November displays widespread but weaker links across the matrix, including south-to-north movements below and above Zanzibar. Both seasons consistently exhibit a very strong (~95%) exchange between two adjacent reefs on Pemba's eastern coast.

This study has represented the first step toward the development of a high-resolution oceanographic model that could help resolve coastal dynamics and of specific areas of interest, such as Pemba and Latham Islands, and the small associated hydrodynamic structures that can influence self-recruitment and connectivity. Overall, the findings have underscored the importance of considering both seasonal and spatial variations in current patterns when designing and managing MPAs, as well as the importance of biological patterns of coral species involved in the studies. The observed exceptions and unique connectivity pathways have highlighted the need for adaptive and dynamic management approaches that account for temporal shifts in ocean currents and provide a more comprehensive understanding of regional marine connectivity.

### **A new APP: the Glider Mission Portal**

The CLIMA VRE has also been used to develop an application dedicated to a set of new ITINERIS marine instruments and that follows one of the final suggestions made in Deliverable 8.3. More specifically, the application has been used to display the trajectories of the JERICO CNR-ISMAR glider missions performed under Activity 5.9 of the project.

A marine glider (Figure 26) is an underwater “gliding vehicle” without a propulsion system, capable of traveling hundreds of kilometers and collecting data even under adverse conditions. It operates silently, with low energy consumption, minimizing environmental impact while ensuring long-term temporal coverage. It is able to surface or dive by adjusting its internal volume (Figure 27), which changes its buoyancy, and it measures various oceanographic variables through continuous descent–ascent cycles. The data collected during each dive are transmitted at every surfacing via a two-way satellite communication system, which enables both near real-time data download and the uploading of new commands to modify navigation parameters. In this way, the glider is technically an Autonomous Underwater Vehicle (AUV), as it is literally guided remotely.

As for the ISSTD demonstrator already introduced in Deliverable 8.13, the main idea of the Glider Mission Portal is to develop an interactive application that does not require any programming skills and thus is meant for users of any kind, including researchers and stakeholders. The Glider Mission Portal serves as a central platform for displaying glider tracks and for downloading their data as they continuously profile the water column, providing high-resolution measurements of key oceanographic variables across large spatial and temporal scales. The portal displays glider locations in time and mission tracks on an interactive map, along with links to the scientific data transmitted via satellite during each mission.

The Glider Mission Portal APP has been designed thanks to the same packages of the ISSTD demonstrator, specifically the XARRAY, BOKEH, HV PLOT and PANEL packages.

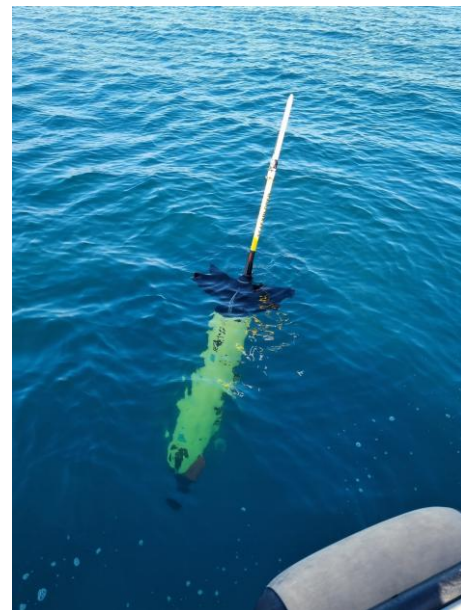
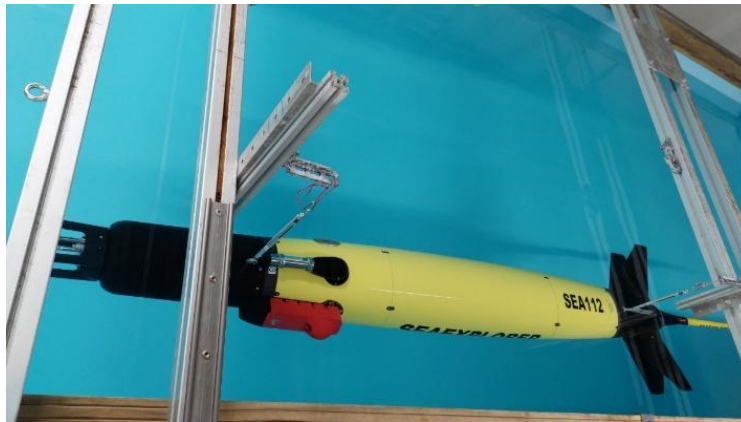


*Figure 26: Images of the JERICO CNR-ISMAR marine gliders acquired thanks to the ITINERIS project in Activity 5.9. Upper panel: the SEA112 (a.k.a. “Pandora”) glider during the ballasting procedure to regulate its asset under seawater. Lower panels: the SEA113 (a.k.a. “Morgana”) glider before the release (left panel) and the recovery (right panel) of one of the missions performed in the northwestern Mediterranean Sea in 2025.*

The reader is referred to the Deliverable 8.13 for their detailed description. Contrarily to the ISSTD demonstrator, the Glider Mission Portal has also used the IPYLEAFLET package.

Ipyleaflet is an interactive mapping library for Python built on top of the popular JavaScript Leaflet library. It enables users to create dynamic geospatial visualizations directly in a Python environment. The package leverages on the ipywidgets package to synchronize Python and JavaScript, allowing a continuous two-way communication between the map displayed and the Python kernel. It supports a wide range of base maps, including OpenStreetMap, satellite imagery, and custom tile servers. Users can easily add interactive markers, polylines, heatmaps, geojson layers, and custom vector data. It

integrates well with scientific libraries like xarray, pandas, and geopandas, and widely used in environmental science, oceanography, and GIS workflows. The package also supports real-time animations, such as updating object positions on the map, making it useful for visualizing model output or tracking moving platforms. Advanced features include drawing tools, layer controls, measure widgets, split-map views, 3D terrain, and the ability to embed Mapbox GL visualizations. Because maps can be embedded in web dashboards, ipyleaflet is increasingly used for decision-support tools and geospatial user interfaces. Its open-source nature and active development community ensure ongoing improvements and compatibility with modern software ecosystems.

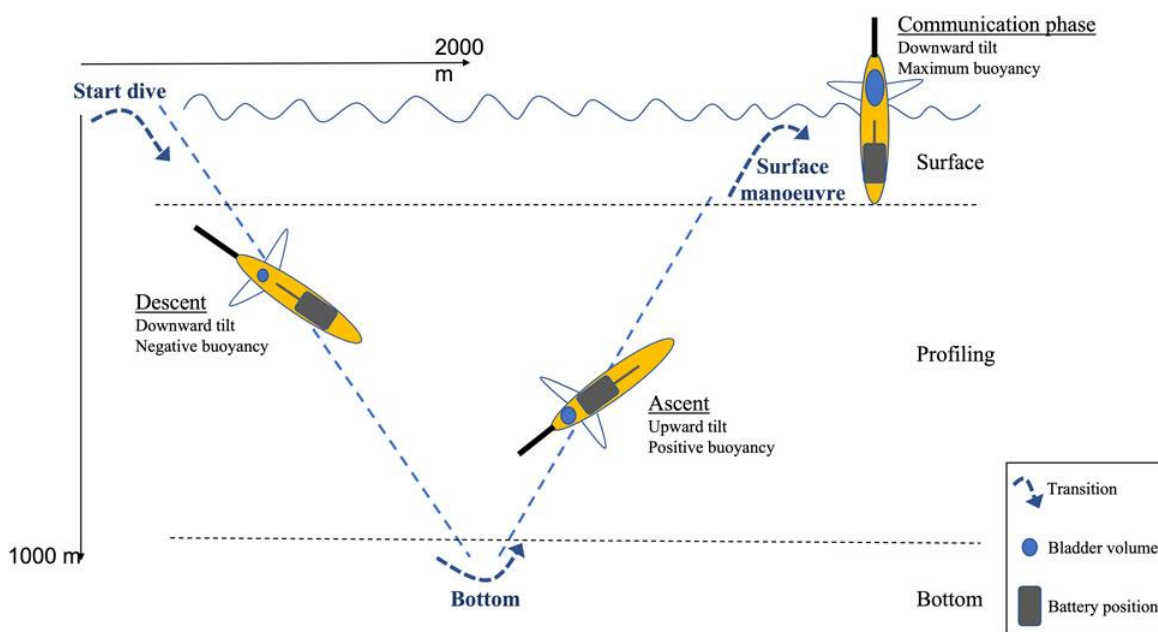


*Figure 27: Schematic diagram of a marine glider dive cycle as shown in Cauchy et al. (2023). The diving pattern is composed of repeated cycles of three successive steady phases: Two profiling phases, descent and ascent, where the glider is collecting scientific measurements, and a communication phase, where the glider stays afloat at the surface communicating with land via satellite and updating its location using GPS.*

As initial step, the application loads a mission track file and displays an interactive glider-mission viewer developed with PANEL and IPYLEAFLET, designed to allow users to explore the trajectory and status of an oceanographic glider during the mission (Figure 28). At the center of the interface, an ipyleaflet map shows the glider's path, with colored line segments indicating its movement over time. The user can pan, zoom, and interact with the map using standard Leaflet controls, including the directional navigation buttons in the upper-right corner and the zoom-in/zoom-out buttons at the bottom-right. A dynamic time indicator at the top updates continuously as the user steps through the mission timeline.

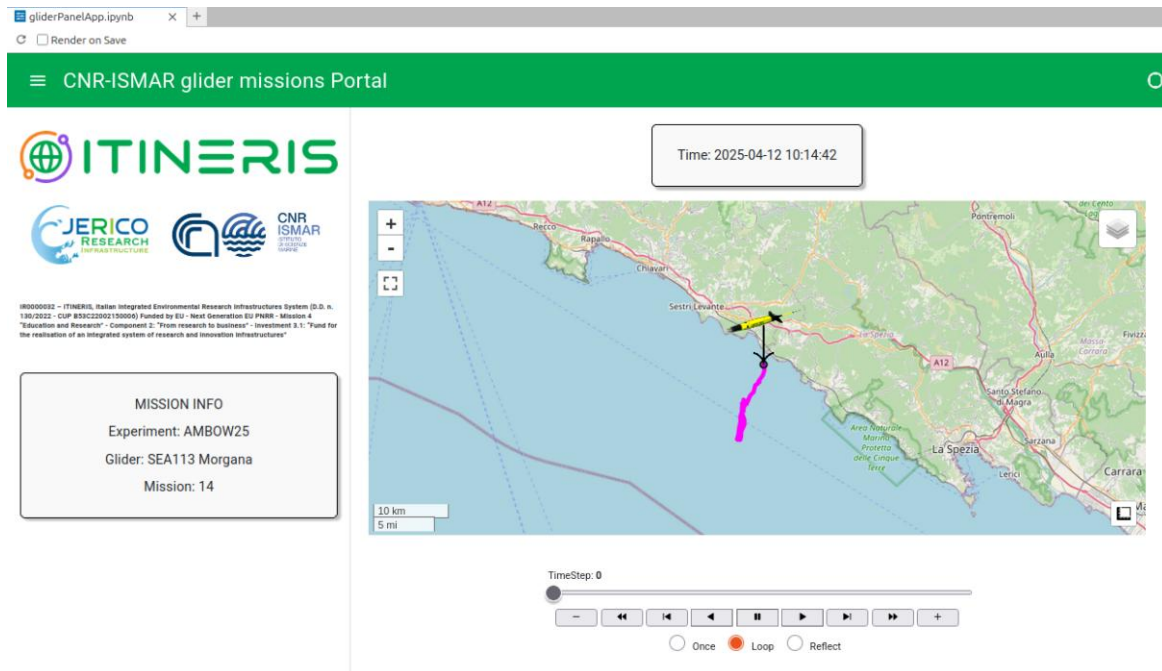


*Figure 28: A comprehensive view of the Glider Mission Portal panel showing all controls and plots as they appear after loading the information for a glider mission. The APP displays in its center the glider's trajectory with full pan and zoom controls, while playback buttons allow step-by-step or animated navigation through the mission. A time slider beneath the map updates the glider position dynamically, enabling exploration of its path over time. The left-side panel includes the project, research infrastructure and institute logos and provides mission metadata, including experiment, vehicle name, and mission number.*

Below the map, a time slider allows users to scroll through individual glider positions recorded during the mission. Each slider movement updates the glider's icon on the map, enabling a frame-by-frame examination of the vehicle's track. Playback buttons (play, pause, step forward/backward, and jump to start/end) support manual or automatic animation of the trajectory, with additional options for looping or reflecting the time sequence for continuous playback. This creates a smooth, interactive visualization of how the glider traveled through the ocean.

On the left side of the page, underneath the project, research infrastructure and institute logos, a mission-information panel provides contextual metadata, including the experiment name, glider model, and mission number. This section helps users quickly identify the dataset they are visualizing without interfering with the map space. Together, these elements make the application a compact yet powerful tool for exploring glider data, combining the flexibility of PANEL layouts with the real-time geographic interactivity of IPYLEAFLET.

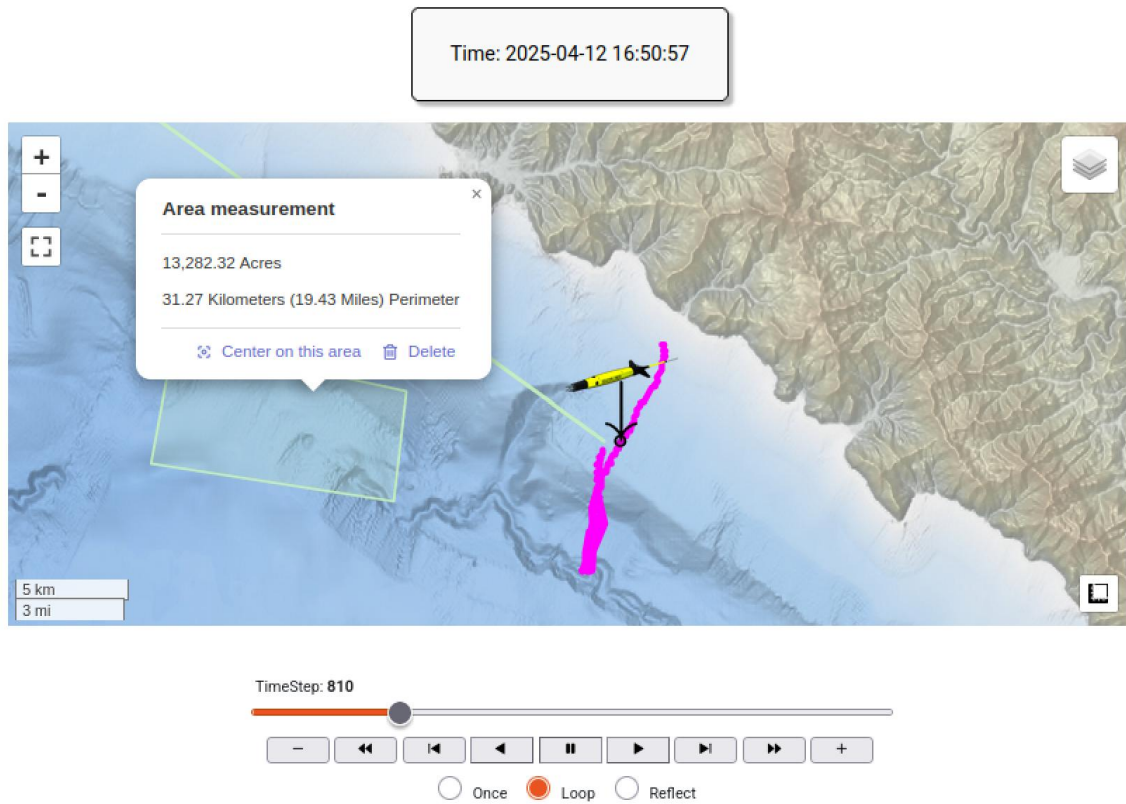


*Figure 30: Zoom in the interactive view of the glider mission with active spatial-measurement tools and synchronized temporal navigation. These additional features extend the functionality described previously by enabling real-time geospatial analysis directly on the mission map.*

Figure 30 illustrates a zoom in the central map of the glider viewer, where users can explore both spatial and temporal dynamics of the vehicle’s trajectory. Users have selected the EMODnet Bathymetry layer to overlay the glider’s path on a detailed bathymetric basemap, improving interpretation of how underwater topography influences the mission route.

A measurement widget is actively displayed, showing calculated area and perimeter values directly on the map, demonstrating the application’s ability to interactively quantify spatial regions. The large time display at the top has synchronized with the slider position, providing immediate temporal context. These features allow fine-grained analysis of glider behavior, including speed changes, turning points, or prolonged sampling in specific regions. By clicking on the glider icon, users are displayed with a link to the ERDDAP server where they can download the mission glider data.

Overall, the APP showcases how the CLIMA VRE can be integrated with the Panel and ipyleaflet packages for an intuitive interaction, temporal navigation, and on-map geospatial analysis.

## 5. CONCLUSIONS

This Deliverable 8.19 concludes the reporting of Activity 8.7 that aimed at developing and implementing a Virtual Research Environment dedicated to climatic variables, the CLIMA VRE.

The development of the CLIMA VRE has fully achieved its original objective: providing an integrated, operational platform capable of supporting advanced climate-related analyses across multiple directions. Its operativity and maturity are demonstrated by the successful design and implementation of the Ligurian Sea Climatic Index (see Section 2), a new climate indicator developed entirely within the VRE, showcasing its ability to handle data ingestion, processing, analysis, and visualization.

Beyond this core achievement, the VRE has proven sufficiently flexible to support habitat mapping efforts and ecological forecasting, as shown by its application to the prediction of invasive species distribution under current and future climate-change scenarios (see Section 3). This work highlights the platform's capacity to merge biological datasets, climatic projections, and machine-learning workflows in a unified environment.

The VRE has also been used to run particle-dispersion simulations aimed at assessing marine connectivity along the Tanzanian coastline (see Section 4), further demonstrating its ability to integrate numerical modelling, oceanographic datasets, and large-scale computation. These three distinct applications confirm that the VRE can support diverse scientific workflows, making it a powerful tool for expert users seeking reproducibility, efficiency, and advanced analytical capacity.

Equally important, the CLIMA VRE has also been used for implementing two interactive applications specifically designed for non-expert users. A new Glider Mission Portal has been integrated into the platform, expanding its capabilities beyond the Italian Sea Surface Temperature Demonstrator (ISSTD) already presented in Deliverable 8.13. This addition complements the existing tools by introducing interactive glider-mission visualization and analysis. Together, the two applications enhance the overall usability of the system as these two tools require no programming skills, providing intuitive access to complex analyses and enabling researchers, stakeholders, and decision-makers to explore results through accessible web interfaces.

All together, the advanced scientific products and the user-friendly applications demonstrate that the CLIMA VRE has evolved into a robust, versatile, and inclusive research environment capable of serving both specialized scientific needs and broader community engagement.

## 6. REFERENCES

- Almany, G.R., Connolly, S.R., Heath, D.D., Hogan, J.D., Jones, G.P., McCook, L.J., Mills, M., Pressey, R.L., and Williamson, D.H., 2009: Connectivity, biodiversity conservation and the design of marine reserve networks for coral reefs. *Coral Reefs*, 28, 339–351. <https://doi.org/10.1007/s00338-009-0484-x>
- Assante M., Candela L., Castelli D., Cirillo R., Coro G., Frosini L., Lelii L., Mangiacrapa F., Pagano P., Panichi G., Sinibaldi F., 2019: Enacting open science by D4Science. *Futur. Gener. Comput. Syst.*, 101, 555-563, <https://doi.org/10.1016/j.future.2019.05.063>
- Assante M., Candela L., Castelli D., Cirillo R., Coro G., Dell'Amico A., Frosini L., Lelii L., Lettere M., Mangiacrapa F., Pagano P., Panichi G., Piccioli T., Sinibaldi F., 2023: Virtual research environments co-creation: The D4Science experience. *Concurrency Computat. Pract. Exper.*, 35 (18), e6925, <https://doi.org/10.1002/cpe.6925>
- Auclair, F., Benshila, R., Bordoï, L., Boutet, M., Brémond, M., Caillaud, M., Cambon, G., Capet, X., Debreu, L., Ducouso, N., et al., 2025: Coastal and Regional Ocean COmmunity model (CROCO), v2.1.0. Zenodo [software]. <https://doi.org/10.5281/zenodo.15064113>
- Azzurro, E., Smeraldo, S., Minelli, A., D'Amen, M., 2022a: Azzurro Ernesto, Smeraldo Sonia, Minelli Annalisa, D'Amen Manuela (2022). ORMEF: a Mediterranean database of exotic fish records. *Sci. Data*, 9 (1), <https://doi.org/10.1038/s41597-022-01487-z>
- Azzurro, E., Smeraldo, S., D'Amen, M., 2022b: ORMEF: Occurrence Records of Mediterranean Exotic Fishes database. [Data set]. Seanoe. <https://doi.org/10.17882/84182>
- Ballesteros, E., 2006: Mediterranean coralligenous assemblages: A synthesis of present knowledge. In R. N. Gibson, R. J. A. Atkinson, and J. D. M. Gordon (Eds), *Oceanography and Marine Biology: An Annual Review*, 44, 123–195. Taylor and Francis, <https://doi.org/10.1201/9781420006391-7>
- Barbet-Massin, M., Jiguet, F., Albert, C.H., and Thuiller, W., 2012: Selecting pseudo-absences for species distribution models: how, where and how many?, *Methods in Ecology and Evolution*, 3 (2), pp. 327–338, <https://doi.org/10.1111/j.2041-210X.2011.00172.x>
- Bianchi, C. N., 2007: Biodiversity issues for the forthcoming tropical Mediterranean Sea. In G. Relini and J. Ryland (Eds.), *Biodiversity in Enclosed Seas and Artificial Marine Habitats*, pp. 7–21, *Developments in Hydrobiology*, volume 193. Springer, Dordrecht. [https://doi.org/10.1007/978-1-4020-6156-1\\_1](https://doi.org/10.1007/978-1-4020-6156-1_1)
- Blunden, J., and Reagan J., 2025: State of the Climate in 2024. *Bull. Amer. Meteor. Soc.*, 106 (8), Si–S513 <https://doi.org/10.1175/2025BAMSStateoftheClimate.1>.
- Bojinski, S., M. Verstraete, T. C. Peterson, C. Richter, A. Simmons, and M. Zemp, 2014: The concept of essential climate variables in support of climate research, applications, and policy. *Bull. Amer. Meteor. Soc.*, 95, 1431–1443, <https://doi.org/10.1175/BAMS-D-13-00047.1>

- Borghini, M., Bryden, H., Schröder, K., Sparnocchia, S., and Vetrano, A., 2014: The Mediterranean is becoming saltier, *Ocean Science*, 10, 693–700, <https://doi.org/10.5194/os-10-693-2014>
- Boucher, O., Servonnat, J., Albright, A. L., Aumont, O., Balkanski, Y., Bastrikov, V., Bekki, S. et al., 2020: Presentation and evaluation of the IPSL-CM6A-LR climate model, *J. Adv. Model. Earth Syst.*, 12 (7), e2019MS002010, <https://doi.org/10.1029/2019ms002010>
- Burt, A.J., Vogt-Vincent, N., Johnson, H., et al., 2024: Connectivity among coral reefs across Seychelles. *Sci Rep* 14, 4936, <https://doi.org/10.1038/s41598-024-55459-x>
- C3S (Copernicus Climate Change Service), 2025: Copernicus: 2024 is the first year to exceed 1.5 °C above pre-industrial level (Press release). Available at: <https://climate.copernicus.eu/copernicus-2024-first-year-exceed-15degc-above-pre-industrial-level>
- Candela L., Castelli D., Pagano P., 2023: The D4Science experience on Virtual Research Environment development. In: *Computing in Science & Engineering*, vol. 25, no. 2, pp. 12-19, <https://doi.org/10.1109/MCSE.2023.3290433>
- Cauchy P., Heywood K.J., Merchant N.D., Risch D., Queste B.Y. and Testor P., 2023: Gliders for passive acoustic monitoring of the oceanic environment. *Front. Remote Sens.* 4, 1106533. <https://doi.org/10.3389/frsen.2023.1106533>
- Cerrano, C., Bavestrello, G., Bianchi, C., Cattaneo-vietti, R., Bava, S., Morganti, C., Morri, C., Picco, P., Sara, G., Schiaparelli, S., Siccardi, A., and Sponga, F., 2000: A catastrophic mass-mortality episode of gorgonians and other organisms in the Ligurian Sea (North-western Mediterranean), *Ecology Letters*, 3, 284–293, <https://doi.org/10.1046/j.1461-0248.2000.00152.x>
- Chefaoui, R. M., Duarte, C. M., and Serrão, E. A., 2018: Dramatic loss of seagrass habitat under projected climate change in the Mediterranean Sea. *Glob Change Biol.*, 24, 4919–4928, <https://doi.org/10.1111/gcb.14401>
- Cherchi, A., Fogli, P. G., Lovato, T., Peano, D., Iovino, D., Gualdi, S., Masina, S., Scoccimarro, E., Materia, S., Bellucci, A., Navarra, A., 2019: Global mean climate and main patterns of variability in the CMCC-CM2 coupled model. *J. Adv. Model. Earth Syst.*, 11, 185–209, <https://doi.org/10.1029/2018MS001369>
- Cossarini, G., Feudale, L., Teruzzi, A., Bolzon, G., Coidessa, G., Solidoro, C., Amadio, C., Lazzari, P., Brosich, A., Di Biagio, V., and Salon, S., 2021: “High-resolution reanalysis of the Mediterranean Sea biogeochemistry (1999–2019)”, *Frontiers in Marine Science*, 8, 741486, <https://doi.org/10.3389/fmars.2021.741486>
- Cyr, F. and Galbraith, P. S., 2021: A climate index for the Newfoundland and Labrador shelf, *Earth System Science Data*, 13, 1807–1828, <https://doi.org/10.5194/essd-13-1807-2021>
- Delandmeter, P., and Van Sebille, E., 2019: The Parcels v2.0 Lagrangian framework: new field interpolation schemes. *Geoscientific Model Development*, 12 (8), 3571–3584. <https://doi.org/10.5194/gmd-12-3571-2019>

- Dobricic, S., and Pinardi, N., 2008: An oceanographic three-dimensional variational data assimilation scheme, *Ocean Modelling*, 22, 89–105, <https://doi.org/10.1016/j.ocemod.2008.01.004>
- Domingues, C.P., Nolasco, R., Dubert, J., and Queiroga, H., 2012: Model-derived dispersal pathways from multiple source populations explain variability of invertebrate larval supply. *PLOS ONE*, 7(4), e35794. <https://doi.org/10.1371/journal.pone.0035794>
- Dunne, J. P., L. W. Horowitz, A. J. Adcroft, P. Ginoux, I. M. Held, J. G. John, J. P. Krasting, et al., 2020: The GFDL Earth System model version 4.1 (GFDL-ESM 4.1): Overall coupled model description and simulation characteristics, *J. Adv. Model. Earth Syst.*, 12 (11). <https://doi.org/10.1029/2019ms002015>
- Estaque, T., Richaume, J., Bianchimani, O., Schull, Q., Mérigot, B., Bensoussan, N., Bonhomme, P., Vouriot, P., Sartoretto, S., Monfort, T., Basthard-Bogain, S., Fargetton, M., Gatti, G., Barth, L., Cheminée, A., and Garrabou, J., 2023: Marine heatwaves on the rise: One of the strongest ever observed mass mortality event in temperate gorgonians, *Global Change Biology*, 29, 6159–6162, <https://doi.org/10.1111/gcb.16931>
- EU-CMEMS (European Union Copernicus Marine Service Information), 2026a: Mediterranean Sea - High Resolution L4 Sea Surface Temperature Reprocessed . Marine Data Store (MDS), <https://doi.org/10.48670/MOI-00173>
- EU-CMEMS (European Union Copernicus Marine Service Information), 2026b: Mediterranean Sea Physics Reanalysis. Marine Data Store (MDS), [https://doi.org/10.25423/CMCC/MEDSEA\\_MULTIYEAR\\_PHY\\_006\\_004\\_E3R1](https://doi.org/10.25423/CMCC/MEDSEA_MULTIYEAR_PHY_006_004_E3R1)
- EU-CMEMS (European Union Copernicus Marine Service Information), 2026c: Mediterranean Sea Biogeochemistry Reanalysis. Marine Data Store (MDS), <https://doi.org/10.48670/mds-00374>
- EU-CMEMS (European Union Copernicus Marine Service Information), 2026d: Global Ocean Physics (GLORYS12V1) Reanalysis. Marine Data Store (MDS), <https://doi.org/10.48670/moi-00021>
- Falossi, M., 2025: A machine learning approach for projections of marine species distributions in the Mediterranean Sea under climate change. Master's thesis, University of Genoa, Genoa, Italy.
- FAO (Food and Agriculture Organization of the United Nations) / GFCM (General Fisheries Commission for the Mediterranean), 2022: Invasive species are changing the nature of the Mediterranean Sea (Press release) Available at the FAO Newsroom: <https://www.fao.org/newsroom/story/Invasive-species-are-changing-the-nature-of-the-Mediterranean-Sea/en>
- Garrabou, J., Ledoux, J.-B., Bensoussan, N., Gómez-Gras, D., and Linares, C., 2021: Sliding Toward the Collapse of Mediterranean Coastal Marine Rocky Ecosystems, in: *Ecosystem Collapse and Climate Change*, pp. 291–324, Springer, Cham, [https://doi.org/10.1007/978-3-235030-71330-0\\_11](https://doi.org/10.1007/978-3-235030-71330-0_11)

- Gawarkiewicz, G., Monismith, S., and Largier, J., 2007: Observing larval transport processes affecting population connectivity: progress and challenges. *Oceanography*, 20(3), 40–53. <https://doi.org/10.5670/oceanog.2007.29>
- Giorgi, F., 2006: Climate change hot-spots. *Geophysical Research Letters*, 33 (8), L08707, <https://doi.org/10.1029/2006GL025734>
- Gómez-Gras, D., Linares, C., Dornelas, M., Madin, J.S., Brambilla, V., Ledoux, J-B., López-Sendino, P., Bensoussan, N. and Garrabou, J., 2021: Climate change transforms the functional identity of Mediterranean coralligenous assemblages, *Ecology Letters*, 24 (5), 1038–1051, <https://doi.org/10.1111/ele.13718>
- Grimsditch, G., Tamelander, J., Mwaura, J., Zavagli, M., Takata, Y., and Gomez, T., 2009: Coral Reef Resilience Assessment of the Pemba Channel Conservation Area, Tanzania. IUCN, Gland, Switzerland, 40 pp. ISBN 978-2-8317-1181-2, [https://www.reefresilience.org/pdf/Tanzania\\_Resilience\\_IUCN.pdf](https://www.reefresilience.org/pdf/Tanzania_Resilience_IUCN.pdf)
- Hedley, J. D., Roelfsema, C. M., Chollett, I., Harborne, A. R., Heron, S. F., Weeks, S., Skirving, W. J., Strong, A. E., Eakin, C. M., Christensen, T. R. L., Ticzon, V., Bejarano, S., & Mumby, P. J., 2016: Remote Sensing of Coral Reefs for Monitoring and Management: A Review. *Remote Sensing*, 8 (2), 118. <https://doi.org/10.3390/rs8020118>
- Hobday, A. J., Alexander, L. V., Perkins, S. E., Smale, D. A., Straub, S. C., Oliver, E. C. J., Benthuisen, J. A., Burrows, M. T., Donat, M. G., Feng, M., Holbrook, N. J., Moore, P. J., Scannell, H. A., Sen Gupta, A., and Wernberg, T., 2016: A hierarchical approach to defining marine heatwaves, *Progress in Oceanography*, 141, 227–238, <https://doi.org/10.1016/j.pocean.2015.12.014>
- Hobday, A. J., Oliver, E. C. J., Gupta, A. S., Benthuisen, J. A., and Burrows, M. T., 2018: Categorizing and Naming Marine Heatwaves, *Oceanography*, 31, 162–173, <https://doi.org/10.5670/oceanog.2018.205>
- IPCC (Intergovernmental Panel on Climate Change), 2021: Climate Change 2021: The Physical Science Basis. Contribution of Working Group I to the Sixth Assessment Report of the Intergovernmental Panel on Climate Change. Cambridge University Press, Cambridge, United Kingdom and New York, NY, USA, 2391 pp. <https://doi.org/10.1017/9781009157896>
- Jimenez, C., Papatheodoulou, M., Resaikos, V., and Petrou, A., 2025: Wholesale destruction inside a Marine Protected Area: Anchoring impacts on sciaphilic communities and coralligenous concretions in the Eastern Mediterranean. *Water*, 17 (14), 2092. <https://doi.org/10.3390/w17142092>
- Katsanevakis S., Poursanidis D., Hoffman R., Rizgalla J., Rothman S.B.-S., Levitt-Barmats Y., Hadjioannou L., Trkov D., Garmendia J. M., Rizzo M., Bartolo A. G., Bariche M., Tomas F., Kleitou P., Schembri P. J., Kletou D., Tiralongo F., Pergent C., Pergent G., Azzurro E., Bilecenoglu M., Lodola A., Ballesteros E., and et al., 2020: Unpublished Mediterranean records of marine alien and cryptogenic species. *BioInvasions Records*, 9 (2), 165–182, <https://doi.org/10.3391/bir.2020.9.2.01>

- Kristiansen, T., Butenschön, M., Peck, M.A., 2024. Statistically downscaled CMIP6 ocean variables for European waters. *Sci. Rep.* 14, 1209, <https://doi.org/10.1038/s41598-024-51160-1>
- Kristiansen, T., and Butenschön, M., 2024: An ensemble of trend preserving statistically downscaled projections for key marine variables under three different future scenarios for the Mediterranean Sea (2.0) [Data set]. Zenodo. <https://doi.org/10.5281/zenodo.10794636>
- Kubin, E., Menna, M., Mauri, E., Notarstefano, G., Mieruch, S., and Poulain, P.-M., 2023: Heat content and temperature trends in the Mediterranean Sea as derived from Argo float data. *Front. Mar. Sci.*, 10, 1271638, <https://doi.org/10.3389/fmars.2023.1271638>
- Lange, M., and van Sebille, E., 2017: Parcels v0.9: prototyping a Lagrangian ocean analysis framework for the petascale age. *Geoscientific Model Development*, 10 (11), 4175–4186. <https://doi.org/10.5194/gmd-10-4175-2017>
- Lazzari, P., and Bolzon, G., 2023: Coupling BFM with OGSTM model. BFM Report series N.4, Release 1.0, February 2023, Trieste, Italy, <http://bfm-community.eu> , pp. 17
- Levin, N., Coll, M., Frascchetti, S., Gal, G., Giakoumi, S., Göke, C., Heymans, J. J., Katsanevakis, S., Mazor, T., Öztürk, B., Rilov, G., Gajewski, J., Steenbeek, J., and Kark, S., 2014): Biodiversity data requirements for systematic conservation planning in the Mediterranean Sea. *Mar. Ecol. Prog. Ser.*, 508, 261–281, <https://doi.org/10.3354/meps10857>
- Lionello, P., and Scarascia, L., 2018: The relation between climate change in the Mediterranean region and global warming, *Reg. Environ. Change*, 18, 1481–1493, <https://doi.org/10.1007/s10113-018-1290-1>
- Lovato, T., D. Peano, M. Butenschön, S. Materia, D. Iovino, E. Scoccimarro, P. G. Fogli, et al., 2022: CMIP6 simulations with the CMCC Earth System Model (CMCC-ESM2), *J. Adv. Model. Earth Syst.*, 14 (3), <https://doi.org/10.1029/2021ms002814>
- Lyons, M. B., M. Roelfsema, C., V. Kennedy, E., M. Kovacs, E., Borrego-Acevedo, R., Markey, K., Roe, M., M. Yuwono, D., L. Harris, D., R. Phinn, S., Asner, G.P., Li, J., E. Knapp, D., S. Fabina, N., Larsen, K., Traganos, D. and J. Murray, N., 2020: Mapping the world's coral reefs using a global multiscale earth observation framework. *Remote Sens. Ecol.*, 6: 557-568. <https://doi.org/10.1002/rse2.157>
- Madec, G., and the NEMO System Team, 2024: NEMO Ocean Engine Reference Manual, Zenodo, <https://doi.org/10.5281/zenodo.1464816>
- Mangubhai, S., and Harrison, P.L., 2006: Seasonal patterns of coral reproduction on equatorial reefs in Mombasa, Kenya. *Proceedings of the 10th International Coral Reef Symposium*, 1, 106–114.
- Mallil, K., Testor, P., Bosse, A., Margirier, F., Houpert, L., Le Goff, H., Mortier, L., and Louanchi, F., 2022: The Levantine Intermediate Water in the western Mediterranean and its interactions with the Algerian Gyres: insights from 60 years of observation, *Ocean Science*, 18, 937–952, <https://doi.org/10.5194/os-18-937-2022>

- Mauritsen, T., J. Bader, T. Becker, J. Behrens, M. Bittner, R. Brokopf, V. Brovkin, et al., 2019: Developments in the MPI-M Earth System Model Version 1.2 (MPI-ESM1.2) and its response to increasing CO<sub>2</sub>, *J. Adv. Model. Earth Syst.*, 11 (4), 998–1038, <https://doi.org/10.1029/2018MS001400>
- McDougall, T. J., and Barker, P. M., 2011: Getting started with TEOS---10 and the Gibbs Seawater (GSW) Oceanographic Toolbox, 28pp., SCOR/IAPSO WG127, ISBN: 978-0-646-55621-5, [https://www.teos-10.org/pubs/Getting\\_Started.pdf](https://www.teos-10.org/pubs/Getting_Started.pdf)
- Mellin, C., MacNeil, M.A., Cheal, A.J., Emslie, M.J., and Caley, M.J., 2016: Marine protected areas increase resilience among coral reef communities. *Ecology Letters*, 19(6), 629–637, <https://doi.org/10.1111/ele.12598>
- Millot, C., 2013: Levantine Intermediate Water characteristics: an astounding general misunderstanding!, *Scientia Marina*, 77, 217–232, <https://doi.org/10.3989/scimar.03518.13A>
- Muhando, C.A., and Mohammed, M.S., 2002: Coral reef benthos and fisheries in Tanzania before and after the 1998 bleaching and mortality event. *Western Indian Ocean Journal of Marine Science*, 1 (1), 43–52.
- Obura, D., Celliers, L., Machano, H., Mangubhai, S., Mohammed, M.S., Motta, H., Muhando, C., Muthiga, N., Pereira, M., and Schleyer, M., 2002: Status of coral reefs in Eastern Africa: Kenya, Tanzania, Mozambique and South Africa. In: Wilkinson, C. (ed.), *Status of Coral Reefs of the World: 2002*. Australian Institute of Marine Science, Townsville, pp. 63–76, [https://www.marinecultures.org/static/files/cots/CORAL\\_REEFS\\_WIO.pdf](https://www.marinecultures.org/static/files/cots/CORAL_REEFS_WIO.pdf)
- Phillips, S. B., Aneja, V. P., Kang, D., and Arya, S. P., 2006: Maximum entropy modeling of species geographic distributions. *Ecol. Model.*, 190 (3-4), 231–259, <https://doi.org/10.1016/J.ECOLMODEL.2005.03.026>
- Randall, C.J., Giuliano, C., Stephenson, B. et al., 2024: Larval precompetency and settlement behaviour in 25 Indo-Pacific coral species. *Commun Biol* 7, 142, <https://doi.org/10.1038/s42003-024-05824-3>
- Ragkousis, M., Zenetos, A., Jamila, B. S., Hoffman, R., Ghanem, R., Taskin, E., Muresan, M., Karpova, E., Slynko, E., Dagli, E., Fortič, A., Surugiu, V., Macic, V., Trkov, D., Rjiba-Bahri, W., Tsiamis, K., Espla, A. A., Petovic, S., Ferrario, J., and et al., 2023: Unpublished Mediterranean and Black Sea records of marine alien, cryptogenic, and neofative species. *BioInvasions Records*, 12 (2), 339–369, <https://doi.org/10.3391/bir.2023.12.2.01>
- Rigal, A., Azaïs, J.-M., and Ribes, A., 2019: Estimating daily climatological normals in a changing climate, *Climate Dynamics*, 53, 275–286, <https://doi.org/10.1007/s00382-018-4584-6>
- Schröder, K., Gasparini, G. P., Tangherlini, M., and Astraldi, M., 2006: Deep and intermediate water in the western Mediterranean under the influence of the Eastern Mediterranean Transient, *Geophysical Research Letters*, 33, <https://doi.org/10.1029/2006GL027121>

- Schröder, K., Josey, S. A., Herrmann, M., Grignon, L., Gasparini, G. P., and Bryden, H. L., 2010: Abrupt warming and salting of the Western Mediterranean Deep Water after 2005: Atmospheric forcings and lateral advection, *Journal of Geophysical Research: Oceans*, 115, <https://doi.org/10.1029/2009JC005749>
- Schultz, L., Wessely, J., Dullinger, S., and Albano, P., 2023: The climate crisis affects Mediterranean marine molluscs of conservation concern. *Diversity and Distributions*, 30, e13805, <https://doi.org/10.1111/ddi.13805>
- Sciascia, R., Magaldi, M. G., and Vetrano, A., 2019: Current reversal and associated variability within the Corsica Channel: The 2004 case study, *Deep Sea Research Part I: Oceanographic Research Papers*, 144, 39–51, <https://doi.org/10.1016/j.dsr.2018.12.004>
- Teruzzi, A., Dobricic, S., Solidoro, C., and Cossarini, G., 2014: A 3-D variational assimilation scheme in coupled transport biogeochemical models: forecast of Mediterranean biogeochemical properties. *J. Geophys. Res. Oceans* 119, 200–217, <https://doi.org/10.1002/2013JC009277>
- Teruzzi, A., Bolzon, G., Salon, S., Lazzari, P., Solidoro, C., and Cossarini, G., 2018: Assimilation of coastal and open sea biogeochemical data to improve phytoplankton modelling in the Mediterranean Sea. *Ocean Model.* 132, 46–60, <https://doi.org/10.1016/j.ocemod.2018.09.007>
- Teruzzi, A., Di Cerbo, P., Cossarini, G., Pascolo, E., and Salon, S., 2019: Parallel implementation of a data assimilation scheme for operational oceanography: the case of the OGSTM-BFM model system. *Comput. Geosci.* 124, 103–114. <https://doi.org/10.1016/j.cageo.2019.01.003>
- Toma, M., Bo, M., Giudice, D., Canese, S., Cau, A., Andaloro, F., Angiolillo, M., Greco, S., and Bavestrello, G., 2022: Structure and status of the Italian red coral forests: What can a large-scale study tell?, *Frontiers in Marine Science*, 9, <https://doi.org/10.3389/fmars.2022.1073214>
- Valli, A., 2024: Dispersal processes and connectivity studies in the marine environment for the realisation of Marine Protected Areas in Tanzania. Master's thesis, University of Genoa, Genoa, Italy.
- van der Ven, R.M., Ratsimbazafy, H.A., and Kochzius, M., 2022: Genetic structure of a broadcast-spawning coral. *Coral Reefs*, 41, 611–624. <https://doi.org/10.1007/s00338-022-02259-4>
- Vichi M., Lovato T., Butenschön M., Tedesco L., Lazzari P., Cossarini G., Masina S., Pinardi N., Solidoro C., and Zavatarelli M., 2023: The Biogeochemical Flux Model (BFM): Equation Description and User Manual. BFM version 5.3. BFM Report series N. 1, Release 1.3, February 2023, Bologna, Italy, <http://bfm-community.eu> , pp. 104
- Vogt-Vincent, N., and Johnson, H., 2022: Winds-M: A 1/50° multidecadal regional simulation of the southwestern Indian Ocean with high frequency surface currents for Lagrangian applications (realistic forcing, 1993–2020), NERC British Oceanographic Data Centre [data set], <https://doi.org/10.5285/BF6F0CFBD09E47498572F21081376702>

- Vogt-Vincent, N.S., Mitarai, S. and Johnson, H.L., 2023: High-frequency variability dominates potential connectivity between remote coral reefs. *Limnol Oceanogr*, 68: 2733-2748. <https://doi.org/10.1002/lno.12455>
- Wilkinson M. D., Dumontier M., Aalbersberg I. J., Appleton G., Axton M., Baak A., Blomberg N., Boiten J.-W., Bonino da Silva Santos L., Bourne P. E., Bouwman J., Brookes A. J., Clark T., Crosas M., Dillo I., Dumon O., Edmunds S., Evelo C. T., et al., 2016: The FAIR guiding principles for scientific data management and stewardship. *Sci. Data*, 3, 160018, <https://doi.org/10.1038/sdata.2016.18>
- WMO (World Meteorological Organization), 2017: WMO Guidelines on the Calculation of Climate Normals – 2017 edition, WMO-No. 1203, World Meteorological Organization, Geneva, Switzerland, <https://library.wmo.int/idurl/4/41106>
- WMO (World Meteorological Organization), IOC-UNESCO (Intergovernmental Oceanographic Commission), ISC (International Science Council), UNEP (United Nations Environment Programme) and C3S (Copernicus Climate Change Service), 2025: The 2022 GCOS ECVs Requirements, GCOS-245, World Meteorological Organization, Geneva, Switzerland, <https://library.wmo.int/idurl/4/58111>
- Zenetos, A., Gofas, S., Verlaque, M., Çinar, M., García Raso, J., Bianchi, C. N., Morri, C., Azzurro, E., Bilecenoglu, M., Frogliã, C., Siokou-Frangou, I., Violanti, D., Sfriso, A., N, G., Giangrande, A., AN, T., Ballesteros, E., Espla, A. A., Mastrototaro, F., and Streftaris, N., 2010: Alien species in the Mediterranean Sea by 2010. A contribution to the application of European Union’s Marine Strategy Framework Directive (MSFD). Part I. Spatial distribution. *Mediterranean Marine Science*, 11, 381–493. <https://doi.org/10.12681/mms.87>
- Zenetos, A., Gofas, S., Morri, C., Rosso, A., Violanti, D., García Raso, J., Çinar, M., Almogi-Labin, A., Ates, A. S., Azzurro, E., Ballesteros, E., Bianchi, C. N., Bilecenoglu, M., Gambi, M. C., Giangrande, A., Gravili, C., Hyams-Kaphzan, O., Karachle, P. (Voula), Katsanevakis, S., & Mineur, F. (2012). Alien species in the Mediterranean Sea by 2012. A contribution to the application of European Union’s Marine Strategy Framework Directive (MSFD). Part 2. Introduction trends and pathways. *Mediterranean Marine Science*, 13, 328–352. <https://doi.org/10.12681/mms.327>